# The remarkably low affinity of CD4/peptide-major histocompatibility complex class II protein interactions

**Short title:** The remarkably low affinity of CD4 for pMHC II

*Peter Jönsson*[a,b]*, *Jennifer Southcombe*[c,d,e]*, *Ana Mafalda Santos*[c,d], *Jiandong Huo*[c,d], *Ricardo A. Fernandes*[c,d], *James McColl*[a], *Melissa Lever*[f], *Edward J. Evans*[c,d], *Alexander Hudson*[c,d], *Veronica T. Chang*[c,d], *Tomáš Hanke*[c], *Andrew Godkin*[h], *Paul D. Dunne*[a], *Mathew H. Horrocks*[a], *Matthieu Palayret*[a], *Gavin R. Screaton*[c], *Jan Petersen*[i,j], *Jamie Rossjohn*[h,i,j], *Lars Fugger*[c,d,g], *Omer Dushek*[f], *Xiaoning Xu*[c]§, *Simon J. Davis*[c,d]§ *and David Klenerman*[a]§

[a] Department of Chemistry, University of Cambridge, Cambridge, CB2 1EW, UK;

[b] Department of Chemistry, Lund University, SE-22100 Lund, Sweden;

[c] MRC Human Immunology Unit, [d] Weatherall Institute of Molecular Medicine, [e] Nuffield Department of Obstetrics and Gynaecology, [f] Sir William Dunn School of Pathology, [g] Nuffield Department of Clinical Neurosciences, Division of Clinical Neurology, University of Oxford, Oxford, OX3 9DS, UK;

[h] Department of Infection and Immunity, School of Medicine, Cardiff University, CF14 4XN, UK;

[i] Infection and Immunity Program and Department of Biochemistry and Molecular Biology, Biomedicine Discovery Institute, Monash University, Clayton, Victoria 3800, Australia;

[j] Australian Research Council Centre of Excellence in Advanced Molecular Imaging, Monash University, Clayton, Victoria 3800, Australia

* These authors contributed equally to this work

§ Corresponding authors:

dk10012@cam.ac.uk, simon.davis@imm.ox.ac.uk, x.xu@imperial.ac.uk

**Keywords:** protein interactions, TCR phosphorylation, adhesion, T-cell activation, binding equilibrium and kinetics

**Classification:** Biological Sciences – Immunology and Inflammation

**Author contributions:** PJ, JS, GRS, XX, SJD, OD and DK designed research; PJ, JS, AMS, RAF, JM, EJE, AH, VTC, MP, ML, JH and PDD performed research; TH, LF, AG, JP, JR and MHH contributed new reagents/analytic tools; PJ analyzed data; PJ, JS, AMS, SJD and DK wrote the paper.

**Abstract.** The αβ T-cell co-receptor CD4 enhances immune responses more than one million-fold in some assays, and yet the affinity of CD4 for its ligand, peptide-major histocompatibility class II (pMHC II) on antigen-presenting cells, is so weak that it was previously unquantifiable. Here, we report that a soluble form of CD4 failed to bind detectably to pMHC II in surface plasmon resonance-based assays, establishing a new upper limit for the solution affinity at 2.5 mM. However, when presented multivalently on magnetic beads, soluble CD4 bound pMHC II-expressing B cells, confirming that it is active and allowing mapping of the native co-receptor binding site on pMHC II. Whereas binding was undetectable in solution, the affinity of the CD4/pMHC II interaction could be measured in two dimensions (2D) using CD4- and adhesion molecule-functionalized, supported lipid bilayers, yielding a 2D dissociation constant, $K_d$, of ~5000 molecules/$\mu m^2$. This value is 2-3 orders of magnitude higher than previously measured 2D $K_d$ values for interacting leukocyte surface proteins. Calculations indicated, however, that CD4/pMHC II binding would increase rates of T-cell receptor (TCR) complex phosphorylation by three-fold via the recruitment of Lck, with only a small, 2-20% increase in the effective affinity of the TCR for pMHC II. The affinity of CD4/pMHC II therefore appears to be set at a value that increases T-cell sensitivity by enhancing phosphorylation, without compromising ligand discrimination.

**Significance statement**

The function of the T-cell co-receptor CD4 presents a long-standing puzzle. Although it is among the most potent modulators of immune responses, CD4 interacts with its binding partner, pMHC II, with previously unmeasurably-low affinity. Here, we set a new upper limit for the solution affinity of CD4 and pMHC II and show that the two-dimensional dissociation constant in supported lipid bilayers is as much as 2-3 orders of magnitude higher than that for other interacting leukocyte surface proteins. These findings extend the known physical limits of functional protein interactions at the cell surface and suggest new ways that T cells may utilize differential receptor affinities during antigen recognition and discrimination.

## Introduction

αβ T cells comprise functionally distinct subsets depending on which transcription factors and which of two co-receptors, CD8 or CD4, they express. $CD8^+$ T-cells respond to peptide agonists presented by major histocompatibility class I molecules (pMHC I) and are cytotoxic, whereas conventional $CD4^+$ cells recognize peptide-MHC class II (pMHC II) and provide "help" defined by the cytokines they secrete (1). Cell adhesion assays explain this functionality insofar as CD8 and CD4 bind directly to pMHC I and pMHC II, respectively (2, 3). CD4 comprises two pairs of V-set and C2-set immunoglobulin superfamily domains, with early mutational data showing that the "top" two domains bind pMHC II (4). Crystal structures of cross-species and affinity-matured CD4/pMHC II complexes suggest that CD4 binds a pocket formed by the α2 and β2 domains of pMHC II (5, 6). The role of co-receptors in heightening T-cell responses is well established. For example, whereas $CD4^+$ T-cells can respond to single pMHC II complexes presented by antigen-presenting cells (APCs), 30 or more complexes are required if CD4 is blocked (7).

How CD4 achieves these effects, however, is incompletely understood. Co-receptors are pivotal in recruiting the kinase Lck to T-cell receptor(TCR)/pMHC complexes (8, 9), but for

reasons that are unclear co-receptor/pMHC interactions are extraordinarily weak. Traditionally, weak protein interactions are characterized using surface plasmon resonance (SPR) measurements, where one protein is tethered to the sensor surface and over it the other is passed at various concentrations. The SPR-based affinity of CD8 for pMHC I is 50 to 200 μM (10). However, SPR has thus far failed to detect interactions between CD4 and pMHC II, setting a lower limit of the dissociation constant, $K_d$, at least two orders of magnitude higher than for typical interacting leukocyte-expressed proteins (5, 10, 11).

Here, we use SPR assays to extend the upper limit of the CD4/pMHC II solution affinity. However, the interactions of proteins in solution may differ from those at contacts between two cells, or between a cell surface and model lipid bilayer (11–14). We therefore also analyzed the two-dimensional (2D) affinity of the CD4/pMHC II interaction for B-cells interacting with supported lipid bilayers (SLBs) containing fluorescently-labelled CD4 and the small T-cell adhesion protein CD2, used to create a physiological context for CD4/pMHC II binding. CD2 is expressed by T cells and binds CD58 on B cells with much higher affinity than the CD4/pMHC II interaction (15, 16). Including CD2 ensured that CD4/pMHC II bonds had time to develop and reduced the risk of biasing the data toward cells with high avidity for CD4 (15).

Other 2D $K_d$ measurements have been made, but only for systems where the average $K_d$ is significantly lower than that of CD4/pMHC II binding (12, 13, 16, 17). Here, we use the method of Zhu et al. (16) to measure the 2D $K_d$ for the CD4/pMHC II interaction, which proves to the best of our knowledge to be the weakest such interaction ever studied. The surface density of CD4 bound to pMHC II on the B cell, *B*, is related to the surface density of free CD4 in the SLB beneath the cell, *F*, by the Zhu-Golan expression:

$$\frac{B}{F} = \frac{N_t \times f}{K_d \times S_{cell}} - \frac{B \times p}{K_d} \qquad \textbf{[1]}$$

where $N_t$ and $f$ are the number and mobile fraction of pMHC II molecules, respectively, $S_{cell}$ is the surface area of the cell and $p$ is the ratio of the SLB/cell contact area to $S_{cell}$. Measurements were also made for rat CD2 and CD48 for comparison and as a test of the CD4/pMHC II results. We finally consider why CD4/pMHC II binding is so weak and develop a mathematical model to investigate how it could affect the stability of TCR/pMHC II complexes and impact on rates of Lck recruitment and TCR phosphorylation. Our findings extend the known physical limits of functional protein interactions at the cell surface.

## Results

**Binding of soluble CD4 to pMHC II.** We first tried to directly measure the binding affinity of CD4 for pMHC II molecules in SPR-based assays. For this, soluble biotinylatable human CD4 (sCD4) was expressed in mammalian cells ((18) see Materials and Methods). sCD4 bound stoichiometrically at distinct epitopes to two different mouse anti-human CD4 antibodies (ADP318 and RPA-T4; see Fig. S1*A*,*B*), and it also bound to HIV-1 gp120 (see Fig. S1*C*), indicating that it was homogeneous and correctly folded. sCD4 was injected at different concentrations at 37 °C over a sensor surface presenting immobilized HLA-

DRB1*01:01/DRA*01 (DR1) pMHC II bound with influenza hemagglutinin (HA) peptide or HLA-A*24:02 (A24) pMHC I bound with a Dengue peptide (Den2) as a negative control (see Fig. 1*A*). The pMHC II proteins bound strongly to L243, a conformation-sensitive, pan anti-human DR antibody (see Fig S2*A*), indicating that the pMHC II was functional. However, even at exceptionally high concentrations of sCD4 (up to 2.5 mM), no significant difference in response was detectable between the control and the pMHC II-containing flow cells (see Fig. 1*A*). Injections at the highest concentration (2.5 mM) at 4 °C (to minimize dissociation) also gave no binding (see Fig. S2*B*). These measurements were repeated with two other pMHC II, i.e. HLA-DRB1*15:01/DRA*01 (DR2) bound with MBP peptide and HLA-DRB1*04:01/DRA*01 (DR4) bound with EBV peptide, with the same outcome (see Fig. S3).

To confirm that sCD4 could bind pMHC II we developed a multivalent binding assay. DR1, the beta chain of which was attached N-terminally to HA peptide and C-terminally to GFP (i.e. HA-DR1-GFP; see Fig. S4*A*), was expressed in HEK 293T cells. Biotinylated sCD4 (sCD4biot) tetramerized with phycoerythrin-labelled streptavidin (SA) bound strongly to HEK 293T cells expressing HIV-1 gp120-GFP, but not to cells expressing HA-DR1-GFP (see Fig. S4*B*). sCD4biot avidity was then increased by attaching it to SA-coated magnetic beads (~50,000 sCD4biot/bead) and used to "pull down" HA-DR1-GFP-expressing cells (Fig. 1*B*; example bead-bound cells are shown in Fig. 1*C*). Three- to four-fold more cells expressing HA-DR1-GFP could be recovered than cells expressing the DR1β chain or GFP-only (see Fig. 1*B*), demonstrating binding of sCD4 to HA-DR1-GFP. However, this was only a quarter of the recoverable gp120-GFP-expressing cells (see Fig. 1*B*), emphasizing the very low affinity of CD4/pMHC II binding. The interaction was sensitive to mutations of residues clustered in the pocket between the α2 and β2 domains used by affinity-matured CD4 to bind DR1 and DR4 (19), *i.e.* βI148, βL158, αT90 and αL92 (see Fig. 2, Fig. S4*C* and SI Text, Section 1). Mutations of residues analogous to those in pMHC I that bind CD8, *i.e.* βE137 and βV142, were disruptive as noted previously (20), due perhaps to indirect effects on the structure of the pocket. Mutations of αK126, αT129 and αT130 at a second site proposed to allow CD4/pMHC II complex oligomerization (21) were without effect, however, implying that CD4 does not bind this region. Overall these data are consistent with native CD4 binding pMHC II at the single site identified in structures of cross-species and affinity-matured CD4/pMHC II complexes, and with binding being undetectable in SPR experiments due to the very low solution affinity of this interaction.

**Binding of B cells to CD4 in lipid bilayers.** SLBs containing different amounts of Alexa Fluor® 647-labelled, lipid-anchored CD4 (400 - 4000 molecules/$\mu m^2$) were used to investigate CD4/pMHC II binding at the B-cell surface at room temperature (22 °C). Raji B-cells were added above the SLB and allowed to bind to the proteins in the SLB. To ensure firm contact, and to position the cell surface at physiologically-relevant distances (22), approximately 400 molecules/$\mu m^2$ of Alexa Fluor® 488-labelled, lipid-anchored CD2 was incorporated in the SLB. Video S1 shows B cells settling on an SLB containing 900 molecules/$\mu m^2$ of CD4 and 400 molecules/$\mu m^2$ of CD2.

Three types of SLB/B-cell contacts formed (see Fig. 3). Clear increases in CD2 fluorescence beneath the cells are observed in all three cases but, for case (i), the CD4 intensity decreases compared to outside the cell whereas in cases (ii) and (iii) it increases slightly (see also Fig. S5).

The distribution of cases is: (i) 22±15%, (ii) 52±12% and (iii) 26±11% (mean value ± one standard deviation from 12 experiments), where, from Fig. S5, case (i) is defined as cells to the left of the kink in the fitted curve, and case (ii) and (iii) as cells on the lower and upper half of the slope, respectively. In case (ii) it is also seen that under the cell, but outside the contact area given by the CD2 image (dotted contour in the bright-field image, Fig. 3), the intensity is significantly lower compared to outside the cell (see also SI Text, Section 2). The reason for this is that unbound CD4 is excluded from the cell-cell contact. Case (i) corresponds to an SLB/B-cell contact where no amount of CD4 binding is discernible. This behaviour is not limited to CD4 binding to B cells: CD4 depletion was observed in SLB contacts formed by pMHC II non-expressing Jurkat cells (see Fig. S6*A*), and rat CD2 added to the SLBs, which does not bind human B-cells, was depleted at B-cell contacts (see Fig. S6*B*). However, in these cases depletion only was observed, and not accumulation as observed for the SLB with CD4/B-cell contacts (see case ii and iii in Fig. 3), indicating that CD4/pMHC II binding was being measured. Ligand depletion observed elsewhere has been attributed to steric crowding at the contact (17). This can significantly affect the analysis of binding affinity using Eq. **1** if not corrected for, especially when $B/F < 1$ (16, 17) (see SI Materials and Methods, Section 2 for details of how compensation was made).

**Zhu-Golan analysis of CD4/pMHC II binding.** The amount of CD4 accumulation under different cells on a given SLB varied considerably (see Fig. S5), with the standard deviation of $B/F$ for each experiment being ~70% of the mean. However, the mean value from different sets of experiments under similar conditions has a much smaller spread and is fairly reproducible (see Fig. 4). The variation therefore results from differences between the cells and their CD4 avidity rather than measurement uncertainty. Plotting the mean value of $B/F$ from each SLB resulted in the data shown in Fig. 4 for CD4/pMHC II binding and for rat CD2 (35 – 1600 molecules/μm$^2$) binding to rat CD48 (either wild-type (WT), or a weakly-binding mutant Q40R (23)). For the latter experiments CD48-transfected Jurkat T-cells were used and ~100 molecules/μm$^2$ of human CD58 was added to the SLBs to position the cells (see Figs. S6*C,D*).

The experimental data were fitted to Eq. **1** with values of $N_t$ and $S_{cell}$ determined as described in the Materials and Methods (see Table 1 for values), assuming a mobile fraction of $f = 1$. The only free parameter to fit is then $K_d$. This gave the following 2D $K_d$ values: 4800 molecules/μm$^2$ for CD4/pMHC II (see also SI Text, Section 3), 38 molecules/μm$^2$ for CD2/CD48 (WT) and 380 molecules/μm$^2$ for CD2/CD48 (Q40R). To validate the analysis we also analysed the rat CD2/CD48 (WT) data using the standard Zhu-Golan method, where the slope of the data in Fig. 4 is used to determine $K_d$ without knowing $N_t$, $f$ and $S_{cell}$ (16). The observation that the two values were the same (38 molecules/μm$^2$) indicated that our method of analysis was approximately valid, at least for the rat CD2/CD48 case. We did not use the Zhu-Golan analysis for all data sets because using the slope to determine the $K_d$ value is less accurate for the weaker interactions since the slow change in $B/F$ vs $B\times p$ is less than, or comparable to, the accuracy of the measurements for those cases. This is less of a problem when fixing $N_t$, $f$ and $S_{cell}$, which gives more accurate values for $K_d$ assuming that the error in choosing $N_t$, $f$ and $S_{cell}$ is not too large.

The 2D $K_d$ value for WT rat CD2/CD48 binding is similar in magnitude, but slightly smaller, than previous measurements (15). The 2D $K_d$ value for the weak-binding Q40R mutant is ten-

fold larger than that for the WT, similar to the ratio in the 3D $K_d$ measurements (see Table 1). These interactions are weak compared to many other protein interactions between T-cells and APCs, as illustrated also by their relatively large 3D $K_d$ values. However, the CD4/pMHC II 2D $K_d$ at 5000 molecules/μm$^2$ is one to two orders of magnitude larger compared to these interactions, three orders of magnitude larger than that for human CD2/CD58 binding (17), and two to three orders of magnitude larger than that for TCR/pMHC interactions (13, 24). The 3D $K_d$ values for the latter interactions is ~10 μM (10, 13, 24, 25), so it can be expected that the 3D $K_d$ for CD4/pMHC II binding should, similar to the 2D $K_d$, be two to three orders of magnitude larger than this value. This is in agreement with a lower limit of 2.5 mM for the 3D $K_d$ of the CD4/pMHC II interaction measured here using SPR, although extrinsic factors such as the average distance between the two cell surfaces could in principle significantly affect binding in 2D vs 3D. Measurements of the CD4/pMHC II 2D $K_d$ were also made at 37 °C. The *B*/*F* ratios from different SLBs were, within the accuracy of the experiments, similar to those at room temperature.

A delimited area of the SLB/B-cell contact was bleached and recovery studied to investigate the dynamic behaviour of the CD4/pMHC II interaction (see Fig. S7). The fluorescence from free and bound CD4 almost completely recovered within 2 minutes indicating that the amount of trapped CD4 in the contact is small compared to the density of mobile molecules. From a fit of the recovery data (see Fig. S7*B*) an average diffusivity of $D = 0.16 \pm 0.06$ μm$^2$/s ($N = 4$) was obtained for CD4 in the contact. This value is ten times smaller than that for free CD4 outside the contact ($1.8 \pm 0.2$ μm$^2$/s; $N = 4$),most likely caused by a higher net drag of the protein in the contact, rather than specific CD4 binding events (see SI Text, Section 4 for details).

**Modelling of the effects of CD4 on TCR/pMHC II stability and phosphorylation rate.** Different mathematical expressions were derived to investigate how the very weak CD4/pMHC II interaction affects T-cell sensitivity and the stability of ternary TCR/pMHC II complexes.

*(i) Effect of CD4 on Lck recruitment to non-phosphorylated TCRs.* CD4-associated Lck (CD4-Lck) can only phosphorylate the TCR complex when it is within a certain area, *A*, around the TCR/pMHC II. It can be assumed that Lck is within area *A* when CD4-Lck binds to pMHC II in a TCR/pMHC II pair, which means that bound CD4-Lck can phosphorylate the TCR/pMHC II complex an extra fraction $R_t/K_c$ of the time (see SI Text, Section 5 for details), where $R_t$ is the density of CD4-Lck and $K_c$ is the 2D $K_d$ of the CD4/pMHC II interaction. This results in the following formula for the overall rate of TCR phosphorylation by CD4-Lck, for which the second term is due to Lck recruitment:

$$k_{\mathrm{p,\,CD4\text{-}Lck/TCR}} = k_{\mathrm{p,\,LCK/TCR}}\left(1 + \sigma / K_c\right) \qquad \textbf{[2]}$$

where $k_{\mathrm{p,\,CD4\text{-}Lck/TCR}}$ and $k_{\mathrm{p,\,Lck/TCR}}$ are the rates of TCR phosphorylation by CD4-Lck and Lck, respectively, and $\sigma = 1/A$ is an effective local concentration corresponding to one molecule within area *A*. The actual size of *A* has not been experimentally determined, but is estimated to be of the order of 100 nm$^2$, corresponding to $\sigma = 10000$ molecules/μm$^2$ (8, 9, 26). This is also comparable to the area occupied by Lck in the CD4-Lck/TCR/pMHC II complex (19). With $K_c = 5000$ molecules/μm$^2$, $k_{\mathrm{p,\,CD4\text{-}Lck/TCR}}$ is a factor of three larger than $k_{\mathrm{p,\,Lck/TCR}}$.

*(ii) Effect of CD4 on the stability and phosphorylation of ternary CD4-Lck/phosphorylated TCR/pMHC II complexes.* Following TCR phosphorylation CD4-Lck can bind phosphorylated tyrosines in the TCR complex (27). To investigate how this can affect the recruitment of Lck and the stability of TCR/pMHC II in the ternary complex, we developed a mathematical model describing the equilibrium distribution of CD4-Lck, pMHC II and phosphorylated TCR (TCR-P) in different binding states (see Fig. S8 and SI Text, Section 6). The number of TCR-P is assumed to be low early in T-cell responses, such that most CD4-Lck molecules are not bound to TCR-P. The increase in effective affinity of TCR for pMHC II, $1/K_{\mathrm{eff}}$, in the presence of CD4 can, under these conditions, be shown to be (see SI Text, Section 6 for details):

$$\frac{1/K_{\mathrm{eff}}}{1/K} = \left(1+\frac{R_{\mathrm{t}}}{K_{\mathrm{l}}}+\frac{R_{\mathrm{t}}\sigma}{K_{\mathrm{c}}K_{\mathrm{l}}}+\frac{R_{\mathrm{t}}K}{K_{\mathrm{c}}K_{\mathrm{l}}}\right)\times\left(1+\frac{R_{\mathrm{t}}}{K_{\mathrm{l}}}\right)^{-1} \approx 1+\frac{R_{\mathrm{t}}(\sigma+K)}{K_{\mathrm{c}}K_{\mathrm{l}}} \qquad \textbf{[3]}$$

where $K_{\mathrm{l}}$ and $K$ are the 2D $K_{\mathrm{d}}$ values for binding of CD4-Lck to TCR-P and TCR-P to pMHC II, respectively. The parameter $\sigma$ corresponds again to the local concentration of bound molecules in the complex (see also Eq. **2**), which for simplicity was set to be equal for all three interactions. It has been assumed in Eq. **3** that both the concentration of pMHC II and $R_{\mathrm{t}}$ are significantly lower than $K_{\mathrm{c}}$. The rightmost expression is approximately valid when $R_{\mathrm{t}}/K_{\mathrm{l}} < 1$. Inserting $\sigma$ = 10000 molecules/μm$^2$, $K_{\mathrm{c}}$ = 5000 molecules/μm$^2$, and $R_{\mathrm{t}}/K_{\mathrm{l}}$ = 0.01 to 0.1 (see SI Text, Section 6 for details on how $R_{\mathrm{t}}/K_{\mathrm{l}}$ is estimated) into Eq. 3 gives an apparent affinity increase of 2% to 20%, respectively, when $K << \sigma$. CD4 will thus only modestly affect the stability of the TCR/pMHC II interaction under these conditions.

Using the same assumptions and parameter values the increase in recruitment of CD4-Lck to TCR-P due to CD4/pMHC II binding can also be estimated. For $K_{\mathrm{l}}$ = 250 molecules/μm$^2$ (28), the fraction of CD4-Lck-associated TCR-P/pMHC II increases by 2.6- and 3.0-fold for $R_{\mathrm{t}}/K_{\mathrm{l}}$ = 0.1 and $R_{\mathrm{t}}/K_{\mathrm{l}}$ = 0.01, respectively (see Eq. **S18**). The subsequent phosphorylation of the TCR complex, as well as phosphorylation of recruited ZAP70, will therefore also be increased by approximately 3-fold (see Eq. **S17**). It should finally be noted that, from Eq. **S17** and Eq. **2** this phosphorylation rate ($k_{\mathrm{p,CD4\text{-}Lck/TCR\text{-}P}}$) is 30-40 times larger (depending on the value for $R_{\mathrm{t}}/K_{\mathrm{l}}$) than the initial rate of phosphorylation, i.e. of the unphosphorylated receptor ($k_{\mathrm{p,CD4\text{-}Lck/TCR}}$ in Eq. **2**).

## Discussion

The binding of CD4 to pMHC II is remarkably weak compared to the interactions of other molecules expressed by T cells and APCs. Here, sCD4 monomers failed to bind pMHC II at concentrations as high as 2.5 mM. Since it is likely to be at least double the highest concentration tested, this sets a new lower limit for the solution $K_{\mathrm{d}}$ of 5 mM. To confirm that this measurement was reliable we established a binding assay wherein, in a highly multivalent form, sCD4 binding to cell-expressed pMHC II could be detected. Using this assay we confirmed that for native CD4 the binding site on pMHC II corresponds to that suggested by crystal structures of cross-species and affinity-matured CD4/pMHC II complexes (5, 6). It can therefore be assumed that native CD4 forms the same “v-shaped” complex that affinity-matured CD4 forms with TCR/pMHC II, wherein contact with the TCR is seemingly precluded

(19). It thus seems very unlikely that the ternary CD4/pMHC II/TCR interaction is stabilised by direct interactions between the extracellular domains of CD4 and the TCR.

To characterize binding in 2D approximating the conditions at T-cell/APC contacts, we studied the interactions of B cells with SLBs containing human CD4 and used CD2 to initially anchor and then position the cell on the SLB at a physiologically relevant distance. Zhu-Golan analysis gave a 2D $K_d$ of ~5000 molecules/$\mu m^2$ for the CD4/pMHC II interaction, the largest value ever reported for protein interactions at the cell surface. This value is two to three orders of magnitude larger than typical interactions between molecules expressed by T cells and APCs, but is still specific since CD4 in SLBs did not interact with cells lacking pMHC II. Photobleaching measurements showed that CD4/pMHC II binding is reversible, and that the mobility of CD4 in the contact is more than ten-fold lower compared to outside the contact. While the 2D off-rate ($k_{off}$) for the CD4/pMHC II interaction could not be determined in the present experiments, it can be estimated to be of the order of 250 $s^{-1}$ (see SI Text, Section 7 for details). With a 2D $K_d$ value of 5000 molecules/$\mu m^2$ this gives a 2D on-rate ($k_{on}$) of 0.05 $\mu m^2 molecules^{-1} s^{-1}$, which is comparable to that measured for protein-protein interactions of higher affinity between T cells and APCs (13, 29). However, the $k_{off}$ is orders of magnitude larger (12, 13, 29).

The 2D $K_d$ value obtained here corresponds to the equilibrium value when two cells, or lipid bilayers with proteins, are held with their surfaces positioned relative to each other at a distance similar to that in the synaptic contact between T cells and APCs. Other techniques involving, *e.g.* micropipettes to periodically bring cells containing the two proteins into contact (12, 30), have been used to study the binding kinetics of single bonds when the cells are not aligned. However, including stronger binding auxiliary molecules to align and position the contacting surface, such as rat CD2/CD48 in this work, would be problematic in pipette-based experiments since the binding kinetics of the auxiliary molecules would dominate the overall signal versus that for the specific CD4/pMHC II interaction. The 2D $K_d$ value obtained for the CD4/pMHC II interaction could be different when T cells contact APCs rather than SLBs containing CD4 and CD2. However, the observation that the CD4/pMHC II interaction is orders of magnitude weaker than typical T-cell/APC protein interactions is expected to hold.

But what are the implications of the very large dissociation constant and how does CD4 so profoundly affect T-cell signalling? The important role of CD4 *in vivo* is believed to be the recruitment of Lck to the TCR (8, 9, 31). The recruited Lck would phosphorylate immune-receptor-tyrosine-based-activation-motifs (ITAMs) constituting the initial step of T-cell activation (8, 9). In agreement with this, Xu and Littman found that T-cell responses were significantly reduced if CD4 could not bind pMHC II, and that this depended on CD4-Lck being able to bind phosphorylated tyrosines in the TCR (27). Hong et al. also recently showed that CD4 has a negligible effect on the affinity and lifetime of TCR/pMHC II complexes, indicating that the primary role of CD4 is not TCR/pMHC II stabilisation (30). To see whether our measured affinity of CD4 to pMHC II fits with these results we undertook numerical calculations to establish whether, in particular, (i) CD4 contributes to initial TCR phosphorylation (see Fig. 5*A*), and (ii) how the CD4/pMHC II interaction affects the effective affinity of the TCR for pMHC II and the recruitment of Lck to previously phosphorylated TCRs (see Fig. 5*B*).

The mathematical expressions showed that despite the very low affinity of CD4 for pMHC II it is sufficiently strong to increase the rate of phosphorylation of both unphosphorylated and previously phosphorylated TCRs up to 3-fold due to the recruitment of Lck. However, the effective affinity of the TCR for pMHC II only increased marginally (2-20%) under the same conditions, in agreement with the experimental observations of Hong et al. (30). This indicates that the decrease in T-cell sensitivity when CD4/pMHC II binding is blocked arises from a reduction in TCR phosphorylation by Lck, rather than from de-stabilization of TCR/pMHC II binding. It should, however, be noted that the increase in Lck recruitment of a factor of 3 is significantly less than the 10-100 fold decrease in sensitivity observed in antibody blocking experiments when calcium and IL-2 signalling are monitored (7, 32). A possible explanation for this is that the increase in phosphorylation is magnified by the exponential lifetime of the TCR/pMHC bond (26) as well as by the requirement for multiple triggering events to act cooperatively in producing calcium fluxes and downstream signalling (33). The derived expressions also showed that the phosphorylation of previously phosphorylated TCRs is significantly, i.e. 30-40 times, faster than the phosphorylation of unphosphorylated TCRs. This results from CD4-Lck binding to TCR-P, explaining the observation by Xu and Littman that T-cell responses are significantly reduced when Lck cannot bind to TCR-P (27). It also indicates that phosphorylation of the first tyrosine(s) in the TCR complex is rate-limiting for TCR phosphorylation.

It needs to be emphasized that these calculations are only approximations and their purpose is to illustrate how, even with the low affinity we have measured, CD4/pMHC II binding can augment T-cell signalling. However, it is also possible that CD4 function and signalling are rather more dependent on prior TCR/pMHC II engagement, because this could facilitate CD4 recruitment (in the ways shown in Fig. S9). Other processes, e.g. phosphorylation by tyrosine kinases not associated with CD4, might also affect initial signalling rates. It is furthermore possible that since the local concentration of CD4-Lck is increased in the immunological synapse (31), this could start to stabilize TCR-P/pMHC II in the synapse according to Eq. **3**, which would also increase sensitivity. It is clear that more experiments are therefore needed to completely understand the role of CD4 in T-cell activation, but our data provides two important new insights. First, the interaction of CD4 with pMHC II is very weak but measurable and specific, and second, at this low affinity, CD4 binding can enhance TCR phosphorylation without significantly stabilizing TCR/pMHC binding. Too low a $K_d$ for the CD4/pMHC II interaction would have detrimental effects on the discrimination of self from non-self peptides, whereas a too high $K_d$ would result in too few interactions with pMHC II molecules for signalling to be enhanced via the delivery of CD4-Lck to the binary TCR/pMHC II complex.

## Materials and Methods

The materials and methods used are summarised below; detailed information is given in the SI.

**Solution affinity and bead-binding experiments.** sCD4 protein, and soluble, biotinylatable forms of DR1/HA (residues 307-318:PKYVKQNTLKLA), DR2/MBP (residues 85-99:ENPVVHFFKNIVTPR), DR4/EBV (residues 627-641:TGGVYHFVKKHVHES) and A24/Den2 (residues 555-564:INYADRRWCF) were produced as described previously (34,

35). For testing for binding to sCD4, the biotinylated pMHC II were immobilized on Biacore streptavidin-coated chips at levels of 1600 RU (DR1/HA), 1750 RU (DR2/MBP) and 1840 RU (DR4/EBV). A24/Den2, a kind gift or Prof. T Dong, was immobilized as a negative control at 1600-1900 RU. The affinities of WT and Q40R-mutated rat CD48 were measured as described previously (23).

For the bead binding assay, HEK 293T cells were transfected with constructs encoding fluorescent HA-DR1-GFP or gp120-GFP as a control (see SI Materials and Methods, Section 1 for details). To generate CD4-coated beads 10 μg biotinylated sCD4 protein was incubated with $6.7\times10^6$ magnetic streptavidin beads M-280 (Dynal biotech). HEK 293T cells were transiently transfected by calcium phosphate precipitation with alpha and beta chain constructs to express WT or mutant HA-DR1-GFP molecules (see Fig. S4), or gp120-GFP controls. Following magnetic "pull-down", cells were either viewed by fluorescence microscopy and counted in duplicate microscope fields or absolute numbers of cells recovered were determined using a hemocytometer.

**2D affinity measurements.** An SLB consisting of 1-palmitoyl-2-oleoyl-*sn*-glycero-3-phosphocholine (POPC) from Avanti Polar Lipids with 5-10 wt% of 1,2-dioleoyl-*sn*-glycero-3-[(N-(5-amino-1-carboxypentyl)iminodiacetic acid)succinyl] (Nickel salt) (DGS-NTA; Avanti Polar Lipids) was formed by vesicle fusion. After formation of the SLB the solution was exchanged with a protein mixture of either: (i) polyhistidine-tagged human CD2 (labelled with Alexa Fluor® 488) and human CD4 (labelled with Alexa Fluor® 647) for the CD4/pMHC II measurements and (ii) polyhistidine-tagged rat CD2 (labelled with Alexa Fluor® 488) and human CD58 (labelled with Alexa Fluor® 647) for the CD2/CD48 measurements.

Raji B-cells or Jurkat cells expressing either WT or weakly binding Q40R mutant CD48 were added to the protein-coupled SLBs and were allowed to settle for ~60 minutes before imaging. Number of proteins on the cell surface, $N_t$, was determined by flow cytometry and Quantibrite analysis with saturating concentrations of PE-conjugated monoclonal antibodies (see SI Materials and Methods, Section 2 for details).

Fluorescence imaging was performed in total internal reflection mode with simultaneous imaging of the sample at 488 nm and 647 nm (see SI Materials and Methods, Section 2 for details of the microscope setup). Images of ~50 cells were acquired for each SLB. SLB protein densities were calculated using fluorescence correlation spectroscopy and the images were analyzed as detailed in the SI Materials and Methods, Section 2 to obtain $B/F$ and $B\times p$. $S_{cell}$ was obtained from a bright-field image of the cell. Photobleaching measurements were performed with the same microscopy setup as described in the SI Materials and Methods, Section 2.

**Acknowledgments.** The authors thank Professor P.A. van der Merwe and Dr Marco Fritzsche for helpful comments on the manuscript and Dr. Hugh Reid for technical advice on pMHC II expression. This work was supported by the Wellcome Trust and the UK Medical Research Council. PJ was supported by grants from the Swedish Research Council (number: 623-2014-6387 and 621-2014-3907). OD is supported by a Sir Henry Dale Fellowship jointly funded by the Wellcome Trust and the Royal Society (Grant Number: 098363).

## References


1. Singer A, Adoro S, Park J-H (2008) Lineage fate and intense debate: myths, models and mechanisms of CD4- versus CD8-lineage choice. *Nat Rev Immunol* 8(10):788–801.
2. Norment AM, Salter RD, Parham P, Engelhard VH, Littman DR (1988) Cell-cell adhesion mediated by CD8 and MHC class I molecules. *Nature* 336(6194):79–81.
3. Doyle C, Strominger JL (1987) Interaction between CD4 and class II MHC molecules mediates cell adhesion. *Nature* 330(6145):256–259.
4. Clayton LK, Sieh M, Pious DA, Reinherz EL (1989) Identification of human CD4 residues affecting class II MHC versus HIV-1 gp120 binding. *Nature* 339(6225):548–551.
5. Wang XX, et al. (2011) Affinity maturation of human CD4 by yeast surface display and crystal structure of a CD4-HLA-DR1 complex. *Proc Natl Acad Sci U S A* 108(38):15960–15965.
6. Wang JH, et al. (2001) Crystal structure of the human CD4 N-terminal two-domain fragment complexed to a class II MHC molecule. *Proc Natl Acad Sci U S A* 98(19):10799–10804.
7. Irvine DJ, Purbhoo MA, Krogsgaard M, Davis MM (2002) Direct observation of ligand recognition by T cells. *Nature* 419(6909):845–849.
8. Artyomov MN, Lis M, Devadas S, Davis MM, Chakraborty AK (2010) CD4 and CD8 binding to MHC molecules primarily acts to enhance Lck delivery. *Proc Natl Acad Sci U S A* 107(39):16916–16921.
9. Stepanek O, et al. (2014) Coreceptor Scanning by the T Cell Receptor Provides a Mechanism for T Cell Tolerance. *Cell* 159(2):333–345.
10. van der Merwe PA, Davis S (2003) Molecular interactions mediating T cell antigen recognition. *Annu Rev Immunol* 21:659–684.
11. Davis SJ, et al. (2003) The nature of molecular recognition by T cells. *Nat Immunol* 4(3):217–224.
12. Huang J, et al. (2010) The kinetics of two-dimensional TCR and pMHC interactions determine T-cell responsiveness. *Nature* 464(7290):932–936.
13. Huppa JB, et al. (2010) TCR-peptide-MHC interactions in situ show accelerated kinetics and increased affinity. *Nature* 463(7283):963–967.
14. Wu Y, Vendome J, Shapiro L, Ben-Shaul A, Honig B (2011) Transforming binding affinities from three dimensions to two with application to cadherin clustering. *Nature* 475(7357):510–513.
15. Dustin ML, et al. (1997) Low affinity interaction of human or rat T cell adhesion molecule CD2 with its ligand aligns adhering membranes to achieve high physiological affinity. *J Biol Chem* 272(49):30889–30898.
16. Zhu D-M, Dustin ML, Cairo CW, Golan DE (2007) Analysis of two-dimensional dissociation constant of laterally mobile cell adhesion molecules. *Biophys J* 92(3):1022–1034.

17. Dustin ML (2009) Supported bilayers at the vanguard of immune cell activation studies. *J Struct Biol* 168(1):152–160.

18. Davis SJ, et al. (1992) Antibody and HIV-1 gp120 recognition of CD4 undermines the concept of mimicry between antibodies and receptors. *Nature* 358(6381):76–9.

19. Yin Y, Wang XX, Mariuzza RA (2012) Crystal structure of a complete ternary complex of T-cell receptor, peptide-MHC, and CD4. *Proc Natl Acad Sci U S A* 109(14):5405–5410.

20. König R, Huang LY, Germain RN (1992) MHC class II interaction with CD4 mediated by a region analogous to the MHC class I binding site for CD8. *Nature* 356(6372):796–798.

21. König R, Shen X, Germain RN (1995) Involvement of both major histocompatibility complex class II alpha and beta chains in CD4 function indicates a role for ordered oligomerization in T cell activation. *J Exp Med* 182(3):779–787.

22. James JR, Vale RD (2012) Biophysical mechanism of T-cell receptor triggering in a reconstituted system. *Nature* 487(7405):64–69.

23. Evans EJ, et al. (2006) Crystal structure and binding properties of the CD2 and CD244 (2B4)-binding protein, CD48. *J Biol Chem* 281(39):29309–29320.

24. Grakoui A, et al. (1999) The immunological synapse: a molecular machine controlling T cell activation. *Science* 285(5425):221–227.

25. Rossjohn J, et al. (2015) T Cell Antigen Receptor Recognition of Antigen-Presenting Molecules. *Annu Rev Immunol* 33(1):169–200.

26. Dushek O, van der Merwe PA (2014) An induced rebinding model of antigen discrimination. *Trends Immunol* 35(4):153–158.

27. Xu H, Littman DR (1993) A kinase-independent function of Lck in potentiating antigen-specific T cell activation. *Cell* 74(4):633–643.

28. Hui E, Vale RD (2014) In vitro membrane reconstitution of the T-cell receptor proximal signaling network. *Nat Struct Mol Biol* 21(2):133–142.

29. Tolentino TP, et al. (2008) Measuring diffusion and binding kinetics by contact area FRAP. *Biophys J* 95(2):920–930.

30. Hong J, et al. (2015) Force-Regulated In Situ TCR-Peptide-Bound MHC Class II Kinetics Determine Functions of CD4+ T Cells. *J Immunol* 195(8):3557–3564.

31. Li Q-J, et al. (2004) CD4 enhances T cell sensitivity to antigen by coordinating Lck accumulation at the immunological synapse. *Nat Immunol* 5(8):791–799.

32. Vidal K, Daniel C, Hill M, Littman DR, Allen PM (1999) Differential requirements for CD4 in TCR-ligand interactions. *J Immunol* 163(9):4811–4818.

33. Huse M, et al. (2007) Spatial and Temporal Dynamics of T Cell Receptor Signaling with a Photoactivatable Agonist. *Immunity* 27(1):76–88.

34. Harkiolaki M, et al. (2009) T Cell-Mediated Autoimmune Disease Due to Low-Affinity Crossreactivity to Common Microbial Peptides. *Immunity* 30(3):348–357.

35. Scally SW, et al. (2013) A molecular basis for the association of the HLA-DRB1 locus, citrullination, and rheumatoid arthritis. *J Exp Med* 210(12):2569–2582.

36. Dushek O, et al. (2008) Effects of intracellular calcium and actin cytoskeleton on TCR mobility measured by fluorescence recovery. *PLoS One* 3(12):e3913.

37. Wu J, et al. (2008) A coupled diffusion-kinetics model for analysis of contact-area FRAP experiment. *Biophys J* 95(2):910–919.

38. Sprague BL, Pego RL, Stavreva DA, McNally JG (2004) Analysis of binding reactions by fluorescence recovery after photobleaching. *Biophys J* 86(6):3473–3495.

39. Altan-Bonnet G, Germain RN (2005) Modeling T cell antigen discrimination based on feedback control of digital ERK responses. *PLoS Biol* 3(11):e356.

40. Kumar GS (2014) *Orban's Oral Histology & Embryology* (Elsevier Health Sciences, New Delhi). 13th Ed.

41. Maroun CR, Julius M (1994) Distinct roles for CD4 and CD8 as co-receptors in T cell receptor signalling. *Eur J Immunol* 24(4):959–966.

42. Nika K, et al. (2010) Constitutively active lck kinase in T cells drives antigen receptor signal transduction. *Immunity* 32(6):766–777.

43. Ballek O, Valečka J, Manning J, Filipp D (2015) The pool of preactivated Lck in the initiation of T-cell signaling: a critical re-evaluation of the Lck standby model. *Immunol Cell Biol* 93(4):384–395.

44. Davis SJ, et al. (1990) High level expression in Chinese hamster ovary cells of soluble forms of CD4 T lymphocyte glycoprotein including glycosylation variants. *J Biol Chem* 265(18):10410–10418.

45. Horrocks MH, et al. (2013) Single-molecule measurements of transient biomolecular complexes through microfluidic dilution. *Anal Chem* 85(14):6855–6859.

46. Johansson B, Höök F, Klenerman D, Jönsson P (2014) Label-free measurements of the diffusivity of molecules in lipid membranes. *Chemphyschem* 15(3):486–491.

47. Hu J, Lipowsky R, Weikl TR (2013) Binding constants of membrane-anchored receptors and ligands depend strongly on the nanoscale roughness of membranes. *Proc Natl Acad Sci U S A* 110(38):15283–15288.

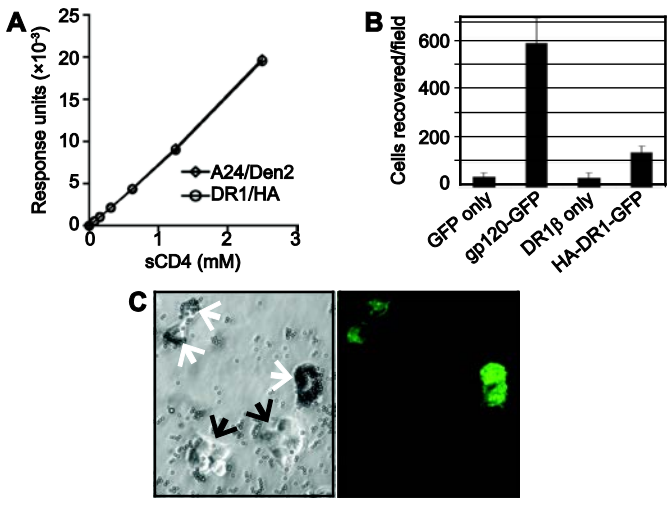

**Figure 1.** The interaction of CD4 with pMHC II in solution is very weak. (*A*) SPR-data showing the response when passing sCD4 over a sensor surface presenting immobilized biotinylated pMHC II molecules (DR1/HA; ○), or a pMHC I molecule (A24/Den2; ◊) as a control. (*B*) Number of isolated pMHC II (HA-DR1-GFP)-expressing HEK 293T cells that bound to biotinylated sCD4-coated beads. Error bars show ± one SEM. (*C*) A bright-field image of cells with bound sCD4-coated beads (*left panel*); white and black arrows identify individual or clustered cells expressing or not expressing HA-DR1-GFP based on a corresponding fluorescence image (*right panel*).

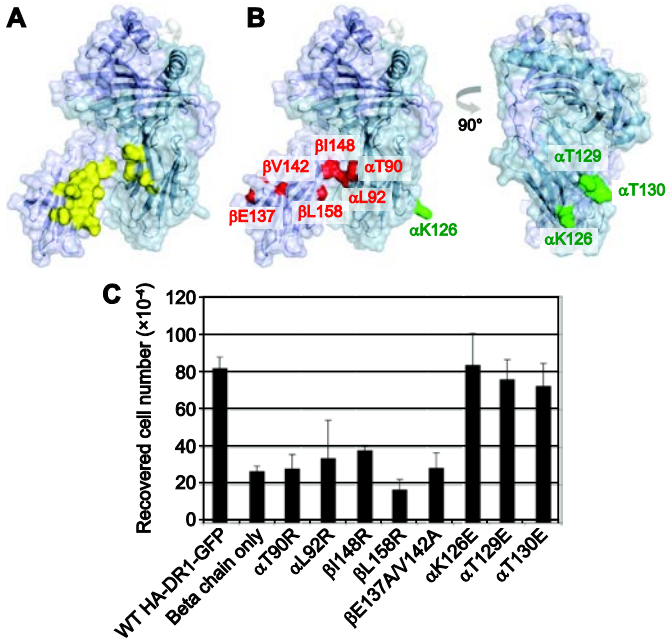


**Figure 2.** The native CD4 binding site of pMHC II. (*A*) The surface of HLA-DR1 (PDB ID code 3S4S) is shown over a ribbon representation of its secondary structure (alpha chain in blue; beta in purple). The surface corresponding to residues that are buried by CD4 in the complex is highlighted in yellow. (*B*) Two orthogonal surface views showing residues whose mutation disrupts binding to CD4 (red), and residues whose mutation has no effect (green). (*C*) Histogram showing the numbers of cells recovered via the binding of CD4-coated magnetic beads, for each of the mutant proteins. Error bars show ± one SD.

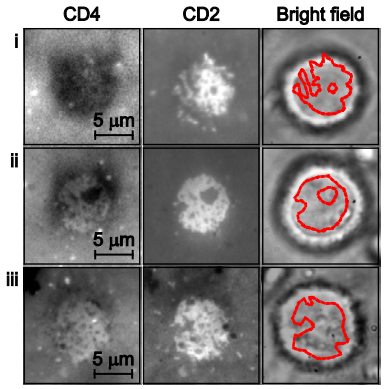


**Figure 3.** Fluorescence images showing different degrees of accumulation of CD4 and CD2 beneath the B cell shown in the bright-field images to the right. The dashed line in the bright-field images shows the contour of the SLB/cell contact identified by CD2 accumulation.

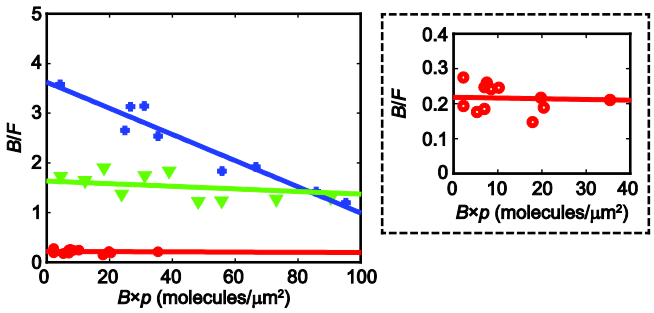


**Figure 4.** Zhu-Golan curves showing the relative accumulation of ligands for three different protein-pair interactions: rat CD2/CD48 (WT; +), rat CD2/CD48 (Q40R; ▼) and CD4/pMHC II (○). The solid lines are linear fits to Eq. **1**, with $N_t \times f$ and $S_{cell}$ fixed, yielding $K_d$ for the different interactions. The panel on the right shows the spread of CD4/pMHC II data across a smaller scale.

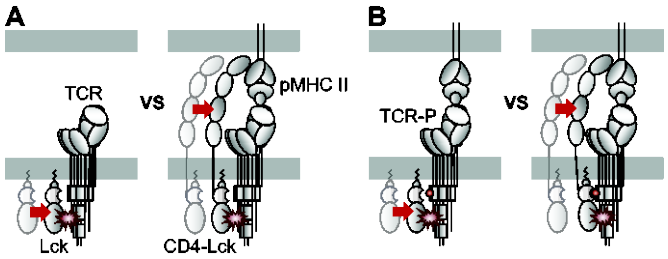


**Figure 5.** The interaction between CD4 and pMHC II increases the phosphorylation rate of TCR, but has less influence on the TCR/pMHC II stability. (*A*) Schematic illustrations showing how binding of CD4-Lck to pMHC II increases the rate of initial TCR phosphorylation. (*B*) Binding of CD4-Lck to TCR-P increases the rate of phosphorylation by recruitment of Lck, while having only a modest effect on the effective affinity of the TCR/pMHC II complex.

**Table 1.** Values for the 2D $K_d$ analysis and corresponding solution (3D) $K_d$ values.

| | **CD4/MHC II**[a] | **CD2/CD48 (WT)** | **CD2/CD48 (Q40R)** |
|---|---|---|---|
| $N_t$ | 570 000 ± 180 000[b] | 95 000 ± 12 000 | 310 000 ± 50 000 |
| $S_{cell}$ | 550 ± 70 μm$^2$ | 690 ± 50 μm$^2$ | 500 ± 80 μm$^2$ |
| **2D $K_d$** | 4800 mol./μm$^2$ | 38 mol./μm$^2$ | 380 mol./μm$^2$ |
| **3D $K_d$** | >2.5 mM | 37 μM | 440 μM |

[a] Protein in the SLB/protein in the contacting cell.

[b] Values are presented as mean ± one SD.

# SUPPORTING INFORMATION

## The remarkably low affinity of CD4/peptide-major histocompatibility complex class II protein interactions

*Peter Jönsson*[a,b]*, *Jennifer Southcombe*[c,d,e]*, *Ana Mafalda Santos*[c,d], *Jiandong Huo*[c,d], *Ricardo A. Fernandes*[c,d], *James McColl*[a], *Melissa Lever*[f], *Edward J. Evans*[c,d], *Alexander Hudson*[c,d], *Veronica T. Chang*[c,d], *Tomáš Hanke*[c], *Andrew Godkin*[h], *Paul D. Dunne*[a], *Mathew H. Horrocks*[a], *Matthieu Palayret*[a], *Gavin R. Screaton*[c], *Jan Petersen*[i,j], *Jamie Rossjohn*[h,i,j], *Lars Fugger*[c,d,g], *Omer Dushek*[f], *Xiaoning Xu*[c]§, *Simon J. Davis*[c,d]§ *and David Klenerman*[a]§

[a] Department of Chemistry, University of Cambridge, Cambridge, CB2 1EW, UK;

[b] Department of Chemistry, Lund University, SE-22100 Lund, Sweden;

[c] MRC Human Immunology Unit, [d] Weatherall Institute of Molecular Medicine, [e] Nuffield Department of Obstetrics and Gynaecology, [f] Sir William Dunn School of Pathology, [g] Nuffield Department of Clinical Neurosciences, Division of Clinical Neurology, University of Oxford, Oxford, OX3 9DS, UK;

[h] Department of Infection and Immunity, School of Medicine, Cardiff University, CF14 4XN, UK;

[i] Infection and Immunity Program and Department of Biochemistry and Molecular Biology, Biomedicine Discovery Institute, Monash University, Clayton, Victoria 3800, Australia;

[j] Australian Research Council Centre of Excellence in Advanced Molecular Imaging, Monash University, Clayton, Victoria 3800, Australia

* These authors contributed equally to this work

§ Corresponding authors:

dk10012@cam.ac.uk, simon.davis@imm.ox.ac.uk, x.xu@imperial.ac.uk

## SI Text

**Section 1. Mutation analysis of the CD4 binding site of DR1.** Using both the multivalent binding assay, in which DR1-expressing cells are recovered with a magnet following their binding of sCD4biot-coated magnetic beads, and *in vitro* mutagenesis, we mapped the region of DR1 bound by CD4. Specifically, we tested whether the crystal structures of the human sCD4/mouse H-2A$^k$ complex (6) or of an affinity-enhanced form of CD4 complexed with DR1 and DR4 (5, 19), in which CD4 binds in a cleft between the α2 and β2 domains of the DR molecules, correctly models the interaction of the native human proteins. We also sought clarification of whether or not CD4 also binds a second site on α2 identified by König et al. that might be responsible for the oligomerization of CD4/pMHC II complexes (20, 21).

We used a "drastic" mutagenesis strategy in which size and and/or charge changes are made to individual side chains in order to maximize the likelihood of significantly altering interface residues. None of the mutations we introduced substantially reduced DR1 expression by the transfectants (see Fig. S4*C*), indicating that the mutations affect surface-exposed residues rather than residues important for folding. Mutations T90R and L92R of α2, and I148R and L158R of β2 each reduced the recovery of HA-DR1-GFP expressing cells by sCD4biot-coated beads more than 50% (see Fig. 2*C*), revealing that human CD4 binds pMHC II in the same way that it binds mouse pMHC II and in the way that the affinity-enhanced form of CD4 binds to DR1 and DR4, *i.e.* in a pocket formed by the α2 and β2 domains of pMHC II. Our data are consistent with the analysis of König et al. (20) wherein the β2 domain double mutant E137A/V142A disrupted CD4 binding (see Fig. 2*C*). However, it now seems likely that this is attributable to indirect effects on the structure of the CD4-binding pocket identified crystallographically. A second binding site was subsequently proposed by König et al. (21) on the grounds that α2 domain mutations prevent CD4 binding. It was proposed that this site mediates CD4/pMHC II complex oligomerization. However, drastic single mutations of a residue in the centre of this region (T129), and of residues immediately adjacent to it (K126 and T130) had no effect on the interaction of CD4 with pMHC II suggesting that this region does not bind CD4 (see Fig. 2*C*). We conclude that the mutations of König et al. (21,22) may have indirectly affected binding and that human pMHC II forms monovalent contacts with CD4 at a site homologous to that identified in the sCD4/H-2A$^k$ and affinity-enhanced sCD4-DR1 and sCD4-DR4 complexes.

**Section 2. Kinetic binding theory.** The surface density of CD4 bound to pMHC II on the B cell, *B*, is related to the surface density of free CD4 in the SLB beneath the cell, *F*, by the Zhu-Golan expression (16):

$$\frac{B}{F} = \frac{N_t \times f}{K_d \times S_{cell}} - \frac{B \times p}{K_d} \qquad \textbf{[S1]}$$

where $N_t$ is the total number of pMHC II molecules on the B cell, $f$ is the mobile fraction of pMHC II molecules, $S_{cell}$ is the surface area of the cell and $p$ is the ratio of the SLB/cell contact area to $S_{cell}$. It has been assumed that the influence binding to immobile receptors has on this expression can be neglected (16).

It can as a first approximation be assumed that the amount of free ligands in the SLB/cell contact area, $F$, is the same as that in the SLB outside the cell contact area, $F^*$. However, as has been observed previously by others, this is not necessarily true and can significantly affect the analysis, especially when $B/F < 1$ (16, 17), resulting in negative $B^*/F^*$ values, where $B^*$ is the value obtained when assuming $F = F^*$. As an example, for the experiments in this work we define $B^*$ as being proportional to the difference in ligand intensity from the cell contact and the intensity from ligands in the SLB outside the cell contact. If free ligands are depleted from the contact, or equivalently if $F < F^*$, then $B^*$ can be negative for weakly binding ligands such as CD4 binding to pMHC II. However, the expressions in Eq. **S2** and Eq. **S4** can be used to convert from the observed ratio $B^*/F^*$ to the actual ratio $B/F$:

$$\frac{B}{F} = \frac{B^*/F^* - \left(B^*/F^*\right)_0}{1 + \left(B^*/F^*\right)_0} \qquad \textbf{[S2]}$$

where the value $(B^*/F^*)_0$ is the ratio of $B^*/F^*$ when no ligands are binding, which is related to $F/F^*$ by:

$$F/F^* = 1 + \left(B^*/F^*\right)_0 \qquad \textbf{[S3]}$$

The surface density of bound CD4 is given by:

$$B = B^* \times \left(1 - \frac{\left(B^*/F^*\right)_0}{B^*/F^*}\right) \qquad \textbf{[S4]}$$

However, in the situation of a brief contact between a T cell and an APC the receptors and ligands on the two opposing cell surfaces will not have time to diffuse over the entire cell surface and reach a steady state concentration profile. For a short, ~1 s, contact the concentration profile in a ~1 $\mu m^2$ T-cell/APC contact can instead be approximated by assuming immobile ligands and receptors resulting in:

$$[\text{CD4/pMHC II}] = \frac{[\text{CD4}] + [\text{pMHC II}] + K_d}{2} - \sqrt{\frac{([\text{CD4}] + [\text{pMHC II}] + K_d)^2}{4} - [\text{pMHC II}] \times [\text{CD4}]} \qquad \textbf{[S5]}$$

where [CD4/pMHC II] is the surface density of CD4 bound to pMHC II molecules and [CD4] and [pMHC II] is the surface density of CD4 and pMHC II, respectively, on the two cells previous to the cell-cell contact. For the situation when either: (i) $K_d$ is larger than both [CD4] and [pMHC II] or (ii) when [pMHC II] >> [CD4], or [CD4] >> [pMHC II], the expression in Eq. **S5** can be approximated with:

$$[\text{CD4/pMHC II}] \approx \frac{[\text{pMHC II}] \times [\text{CD4}]}{[\text{CD4}] + [\text{pMHC II}] + K_d} \approx \frac{[\text{pMHC II}] \times [\text{CD4}]}{K_d} \qquad \textbf{[S6]}$$

where the second equality is valid when $K_d$ >> [CD4] + [pMHC II]. It also follows that if $K_d$ >> [CD4] + [pMHC II] then the fraction of pMHC II molecules that have CD4 bound will be

independent on the actual number of pMHC II. The number of CD4 binding events per second to a single pMHC II molecule is under these conditions given by:

$$n(\text{CD4/pMHC II}) = k_{\text{off}} \frac{[\text{CD4/pMHC II}]}{[\text{pMHC II}]} \approx k_{\text{on}}[\text{CD4}] \qquad \textbf{[S7]}$$

where the last expression is approximately valid when $K_d$ >> [CD4] + [pMHC II].

**Section 3. Accuracy of the CD4/pMHC II 2D $K_d$.** The curve fit to the CD4/pMHC II data in Fig. 4 yields that $K_d$ is between 4200 to 5300 molecules/μm$^2$ with 95% confidence. However, this does not allow for possible errors in choosing $(B^*/F^*)_0$ or errors in averaging the cell data to one value for each SLB. A spread in $N_t$ and $S_{cell}$ depending on cell cycle and the protein turnover will also add to the uncertainty, as will the assumption that $f$ = 1, which might be lower for the present experiments, even though it has in previous studies been observed to be relatively high, and close to one, for similar systems (16, 36). The obtained value of the 2D $K_d$ should therefore only be seen as an order of magnitude estimate of the CD4/pMHC II 2D $K_d$.

**Section 4. Measure of CD4 turnover using photobleaching.** Equation **S1** assumes that the CD4/pMHC II interaction has reached equilibrium. However, CD4 is constantly detaching from and rebinding the pMHC II. This can be observed by photobleaching an area of the SLB/cell contact (24, 29, 37). Fluorescence recovery will, in addition to the sizes of the contact and bleached region, depend on the diffusivity of CD4 both in the contact and in the SLB, and the on- and off-rates for CD4/pMHC II binding (37). Fluorescence recovery after photobleaching was used to study the mobility of CD4 in the SLB/B-cell contact. A delimited area in the contact was bleached and the subsequent recovery of fluorescently-labelled CD4 studied (see Fig. S7). The solid line in Fig. S7*B* is a fit of the recovery giving an average diffusivity of $D$ = 0.16±0.06 μm$^2$/s ($N$ = 4) for CD4 in the contact. This value is ten times smaller compared to the diffusivity of free CD4 outside of the contact, which was 1.8±0.2 μm$^2$/s ($N$ = 4). A reduction in $D$ of similar magnitude has been observed for other proteins in SLB/cell contacts (29).

The recovery will also be affected by the diffusivity outside of the contact, but since the bleached region is mainly confined to the contact area this effect has only a minor influence. The recovery can also depend on the binding parameters of the CD4/pMHC II interaction, *i.e.* the kinetics of binding (37). If the diffusivity is slow compared to the unbinding of the ligand, i.e. if $1/k_{off} > w^2/4D$, where $k_{off}$ is the off-rate and $w$ the Gaussian radius of the bleached area at $t$ = 0, then the recovery will be affected by the binding kinetics and $D$ will no longer only be a measure of the diffusivity of CD4. However, for this to be the case in the current experimental range the off-rate has to be smaller than 0.07 s$^{-1}$. This value is much lower than values obtained for typical T-cell/B-cell protein interactions in solution (13, 29), and single molecule studies in 2D (12, 13). The weak CD4/pMHC II interaction can thus be expected to have a $k_{off}$ much larger than 0.07 s$^{-1}$ and recovery should mainly be governed by diffusion in the contact. However, it has previously been observed that the 2D $k_{off}$ values obtained from photobleaching experiments can be considerably lower than the values measured in solution, due perhaps to

increased rebinding, and Tolentino et al. obtained a kinetic off-rate of 0.07 $s^{-1}$ for rat CD2/CD58 binding (29). It is therefore possible that the recovery is affected by binding kinetics, but due to the small amounts of bound CD4 and the slow recovery in the current experiments this is hard to quantify with certainty from our data. Multiple rebinding of CD4 to pMHC II during the recovery can also result in a drop in diffusivity. The effective diffusion coefficient, $D_{\mathrm{eff}}$, will in this case be given by (38):

$$D_{\mathrm{eff}} = D \times \left(1 + B/F\right)^{-1} \qquad \textbf{[S8]}$$

However, with $B/F$ in the range 0.2 - 0.25 for the CD4/pMHC II interaction this would only give a reduction in the diffusivity by ~20%. Thus, the tenfold drop in diffusivity of CD4 in the SLB/cell contact is more likely to be caused by a higher net drag of the protein in the contact, rather than caused by specific CD4 binding events.

**Section 5. Recruitment of CD4-Lck to non-phosphorylated TCR/pMHC II.** CD4-Lck can only phosphorylate the TCR complex when it is within a certain area, $A$, around the TCR/pMHC II. For randomly moving molecules there will on average be $A \times R_t$ molecules in this area, where $R_t$ is the density of CD4-Lck. If $A \times R_t < 1$ this corresponds to the fraction of time a CD4-Lck molecule is close enough to phosphorylate the TCR. It can be assumed that Lck is within area $A$ when CD4-Lck binds to pMHC II in a TCR/pMHC II pair, which means that bound CD4-Lck can phosphorylate the TCR/pMHC II complex an extra fraction $R_t/K_c$ of the time (see Eq. **S6**), where $K_c$ is the 2D $K_d$ of the CD4/pMHC II interaction. This assumes that both $R_t$ and the amount of pMHC II is much less than $K_c$, and for a general expression Eq. **S5** should be used. Combining these two expressions results in the formula in Eq. **2**.

**Section 6. Equilibrium models to describe the distribution of CD4-Lck, TCR-P and pMHC II.** We consider an equilibrium model consisting of the different states depicted in Fig. S8. Only the effect of Lck molecules associated with CD4 (CD4-Lck) are considered. The parameters $K_c$, $K_l$ and $K$ are the 2D $K_d$ values for CD4-Lck to pMHC II, CD4-Lck to TCR and TCR to pMHC II, respectively. The parameters $K_c^* = K_c/\sigma$, $K_l^* = K_l/\sigma$ and $K^* = K/\sigma$ are effective 2D $K_d$ values for (re)binding of the same protein pairs in the ternary complex. The parameter $\sigma$ corresponds to the local concentration of the protein molecules upon rebinding in the ternary complex, which as an order of magnitude approximation have been set equal for all three interactions. The parameter $\sigma$ can also be defined as $1/A$, where $A$ is the area within which the molecules have to be to be able to interact. The total surface density of pMHC II, CD4-Lck and phosphorylated TCR (TCR-P) is designated $P_t$, $R_t$ and $T_t$, respectively, and the unbound fraction of these molecules are designated $P_f$, $R_f$ and $T_f$. It is assumed that in the early stages of T-cell activation the fraction of TCR-P is much lower than the total amount of CD4-Lck. The influence of CD4, without Lck, binding to pMHC II is neglected in the model due to the low affinity between CD4 and pMHC II. From the density of free pMHC II, free TCR-P and free CD4-Lck in the T-cell/APC contact, and the equilibrium relations between the different states in Fig. S8, the following three coupled equations are obtained:

$$P_\mathrm{f} = P_\mathrm{t} - \left(X + U + Q + W + 2S + V + Y\right) \Leftrightarrow$$
$$P_\mathrm{f}\left(1 + \frac{R_\mathrm{f}}{K_\mathrm{c}}\right) = P_\mathrm{t} - \frac{T_\mathrm{f} P_\mathrm{f}}{K}\left(1 + \frac{R_\mathrm{f}}{K_\mathrm{l}} + \frac{R_\mathrm{f}\sigma}{K_\mathrm{c}K_\mathrm{l}} + \frac{R_\mathrm{f}}{K_\mathrm{c}} + 2\frac{P_\mathrm{f}}{K_\mathrm{c}}\frac{R_\mathrm{f}}{K_\mathrm{l}} + \frac{R_\mathrm{f}K}{K_\mathrm{c}K_\mathrm{l}}\right) \quad \textbf{[S9]}$$

$$T_\mathrm{f} = T_\mathrm{t} - \left(X + U + Q + W + S + V + Z\right) \Leftrightarrow$$
$$T_\mathrm{f}\left(1 + \frac{R_\mathrm{f}}{K_\mathrm{l}}\right) = T_\mathrm{t} - \frac{T_\mathrm{f} P_\mathrm{f}}{K}\left(1 + \frac{R_\mathrm{f}}{K_\mathrm{l}} + \frac{R_\mathrm{f}\sigma}{K_\mathrm{c}K_\mathrm{l}} + \frac{R_\mathrm{f}}{K_\mathrm{c}} + \frac{P_\mathrm{f}}{K_\mathrm{c}}\frac{R_\mathrm{f}}{K_\mathrm{l}} + \frac{R_\mathrm{f}K}{K_\mathrm{c}K_\mathrm{l}}\right) \quad \textbf{[S10]}$$

$$R_\mathrm{f} = R_\mathrm{t} - \left(U + Q + W + S + V + Y + Z\right) \Leftrightarrow$$
$$R_\mathrm{f}\left(1 + \frac{P_\mathrm{f}}{K_\mathrm{c}} + \frac{T_\mathrm{f}}{K_\mathrm{l}}\right) = R_\mathrm{t} - \frac{T_\mathrm{f} P_\mathrm{f}}{K}\left(\frac{R_\mathrm{f}}{K_\mathrm{l}} + \frac{R_\mathrm{f}\sigma}{K_\mathrm{c}K_\mathrm{l}} + \frac{R_\mathrm{f}}{K_\mathrm{c}} + \frac{P_\mathrm{f}}{K_\mathrm{c}}\frac{R_\mathrm{f}}{K_\mathrm{l}} + \frac{R_\mathrm{f}K}{K_\mathrm{c}K_\mathrm{l}}\right) \quad \textbf{[S11]}$$

The density of TCR-P molecules bound to pMHC II, $n_{\mathrm{T+P}}$, is given by:

$$n_{\mathrm{T+P}} = X + U + Q + W + S + V = \frac{T_\mathrm{f} P_\mathrm{f}}{K}\left(1 + \frac{R_\mathrm{f}}{K_\mathrm{l}} + \frac{R_\mathrm{f}\sigma}{K_\mathrm{c}K_\mathrm{l}} + \frac{R_\mathrm{f}}{K_\mathrm{c}} + \frac{P_\mathrm{f}}{K_\mathrm{c}}\frac{R_\mathrm{f}}{K_\mathrm{l}} + \frac{R_\mathrm{f}K}{K_\mathrm{c}K_\mathrm{l}}\right) \quad \textbf{[S12]}$$

and the fraction of TCR-P molecules binding pMHC II is then:

$$\frac{n_{\mathrm{T+P}}}{T_\mathrm{t} - n_{\mathrm{T+P}}} = \frac{P_\mathrm{f}}{K}\left(1 + \frac{R_\mathrm{f}}{K_\mathrm{l}} + \frac{R_\mathrm{f}\sigma}{K_\mathrm{c}K_\mathrm{l}} + \frac{R_\mathrm{f}}{K_\mathrm{c}} + \frac{P_\mathrm{f}}{K_\mathrm{c}}\frac{R_\mathrm{f}}{K_\mathrm{l}} + \frac{R_\mathrm{f}K}{K_\mathrm{c}K_\mathrm{l}}\right) \times \left(1 + \frac{R_\mathrm{f}}{K_\mathrm{l}}\right)^{-1} \quad \textbf{[S13]}$$

The density of CD4-Lck molecules bound to TCR/pMHC II complexes, $n_{\mathrm{R/T+P}}$, is given by:

$$n_{\mathrm{R/T+P}} = U + Q + W + S + V = \frac{T_\mathrm{f} P_\mathrm{f}}{K}\left(\frac{R_\mathrm{f}}{K_\mathrm{l}} + \frac{R_\mathrm{f}\sigma}{K_\mathrm{c}K_\mathrm{l}} + \frac{R_\mathrm{f}}{K_\mathrm{c}} + \frac{P_\mathrm{f}}{K_\mathrm{c}}\frac{R_\mathrm{f}}{K_\mathrm{l}} + \frac{R_\mathrm{f}K}{K_\mathrm{c}K_\mathrm{l}}\right) \quad \textbf{[S14]}$$

which combined with Eq. **S12** gives the fraction of TCR/pMHC II complexes with CD4-Lck bound:

$$\frac{n_{\mathrm{R/T+P}}}{n_{\mathrm{T+P}}} = \frac{R_\mathrm{f}}{K_\mathrm{l}}\left(1 + \frac{\sigma}{K_\mathrm{c}} + \frac{K_\mathrm{l}}{K_\mathrm{c}} + \frac{P_\mathrm{f}}{K_\mathrm{c}} + \frac{K}{K_\mathrm{c}}\right) \times \left(1 + \frac{R_\mathrm{f}}{K_\mathrm{l}} + \frac{R_\mathrm{f}\sigma}{K_\mathrm{c}K_\mathrm{l}} + \frac{R_\mathrm{f}}{K_\mathrm{c}} + \frac{P_\mathrm{f}}{K_\mathrm{c}}\frac{R_\mathrm{f}}{K_\mathrm{l}} + \frac{R_\mathrm{f}K}{K_\mathrm{c}K_\mathrm{l}}\right)^{-1}$$
**[S15]**

Some approximations to the expressions presented above can be made under the present conditions. Equation **S15** can, when $P_\mathrm{t}$ and $R_\mathrm{t}$ << $K_\mathrm{c}$ and $T_\mathrm{t}$ << $R_\mathrm{t}$ (or when $R_\mathrm{f}$ ~ $R_\mathrm{t}$), approximately be written:

$$\frac{n_{\mathrm{R/T+P}}}{n_{\mathrm{T+P}}} \approx \frac{R_\mathrm{t}}{K_\mathrm{l}}\left(1 + \frac{\sigma}{K_\mathrm{c}} + \frac{K_\mathrm{l}}{K_\mathrm{c}} + \frac{K}{K_\mathrm{c}}\right) \times \left(1 + \frac{R_\mathrm{t}}{K_\mathrm{l}} + \frac{R_\mathrm{t}\sigma}{K_\mathrm{c}K_\mathrm{l}} + \frac{R_\mathrm{t}K}{K_\mathrm{c}K_\mathrm{l}}\right)^{-1} \quad \textbf{[S16]}$$

For the situation when $K_l \rightarrow \infty$, corresponding to non-phosphorylated TCRs, Eq. **S16** simplifies to $n_{R/T+P}/n_{T+P} = R_t/K_c$ equivalent to the fraction of CD4 bound to pMHC II given by Eq. **S6**. The effective phosphorylation rate of TCR-P by CD4-Lck, $k_{p,\,CD4\text{-}Lck/TCR\text{-}P}$, can be estimated from Eq. S**16** as:

$$k_{p,CD4-Lck/TCR-P} = k_{p,Lck/TCR}\left(1+\frac{n_{R/T+P}}{n_{T+P}}\frac{\sigma}{R_t}\right) \qquad \textbf{[S17]}$$

where $k_{p,\,Lck/TCR}$ is the phosphorylation rate of TCR by Lck (see also Eq. **2**).

The increase in the fraction of TCR-P/pMHC II with Lck due to the CD4/pMHC II interaction is under these conditions:

$$\left(\frac{n_{R/T+P}}{n_{T+P}}\right)_{CD4-Lck}\Bigg/\left(\frac{n_{R/T+P}}{n_{T+P}}\right)_{only\ Lck} \approx \frac{(1+(\sigma+K_l+K)/K_c)\times(1+R_t/K_l)}{(1+(1+(\sigma+K)/K_c)R_t/K_l)} \qquad \textbf{[S18]}$$

Equation **S13** can under the same conditions as for Eq. **S16** be written:

$$\frac{1}{K_{eff}} = \frac{n_{T+P}}{(T_t-n_{T+P})P_f} \approx \frac{1}{K}\left(1+\frac{R_f}{K_l}+\frac{R_f\sigma}{K_cK_l}+\frac{R_fK}{K_cK_l}\right)\times\left(1+\frac{R_f}{K_l}\right)^{-1} \qquad \textbf{[S19]}$$

where $1/K_{eff}$ under these conditions corresponds to the effective affinity of TCR-P to pMHC II. Equation **S19** can be used to estimate the increase in affinity of TCR-P to pMHC II due to CD4.

Flow-cytometric analysis was used to give totals of 34 000 and 100 000 for the number of CD4 and pMHC II receptors expressed by naïve T- and B-cells, respectively. A total surface area of ~200 μm$^2$ for both cell types ($S_{cell} = 1.8\times\pi d^2$ (16), where $d$ = 6 μm is the cell diameter (39, 40)) gives a CD4 density of 170 molecules/μm$^2$ and pMHC II density of 500 molecules/μm$^2$. Both $R_t$ and $P_t$ is thus significantly smaller than $K_c$ = 5000 molecules/μm$^2$, in agreement with the assumptions leading to Eqs. **S16**, S**18** and **S19**. If it is assumed that 40% of the CD4 molecules are coupled with Lck (41), and that between 2% and 40% of the CD4-Lck are constitutively active (42, 43), then for $K_l$ = 250 molecules/μm$^2$ (28) we get $R_t/K_l \approx 0.01$ to 0.1. This is comparable to theoretical values of $R_t/K_l$ = 0.01 used in previous estimates of the stabilizing effects of CD4/pMHC II interactions (8). Inserting $R_t/K_l$ = 0.01 and 0.1 into Eq. **S19** with $\sigma$ = 10000 molecules/μm$^2$ and $K_c$ = 5000 molecules/μm$^2$, gives an apparent affinity increase of 2% and 20%, respectively, when $K << \sigma$. The same values inserted into Eq. **S18**, with $K_l$ = 250 molecules/μm$^2$, gives an increase in the fraction of TCR-P/pMHC II with Lck of 2.6 to 3.0. CD4-Lck binding to TCR-P will also increase the recruitment of CD4 compared to when it is binding only pMHC II. From Eqs. S**6** and S**16** it follows that CD4 is recruited ~50-fold more efficiently to TCR-P/pMHC II compared to pMHC II alone, although the effective increase will be less because only a fraction of the CD4 is likely associated with constitutively active Lck and thus able to bind TCR-P.

**Section 7. Estimation of kinetic rate constants.** The $k_{off}$ value for the CD4/pMHC II interaction could not be determined in the present study, and so it is unclear whether the high

$K_d$ is due to a low $k_{on}$ value or a high $k_{off}$ value, or a combination of both. However, Wang et al. used affinity-maturation to produce a form of CD4 that bound pMHC II with a 3D $k_{off}$ of ~0.5 $s^{-1}$ and a 3D $K_d$ of 10 μM (5). Conversion of the 3D $K_d$ to a 2D $K_d$ using the relationship obtained experimentally for the rat CD2/CD48 interactions in Table 1 gives a 2D $K_d$ of approximately 10 molecules/$\mu m^2$ for the affinity-matured interaction. This should, however, only be considered as an order of magnitude estimate since the ratio between 3D and 2D $K_d$ can vary substantially between different protein molecules (11–14). If it is furthermore assumed that the mutations made by Wang et al. mostly affect $k_{off}$, based on the observation that the primary effect of the mutations was to improve the geometric fit of CD4 to pMHC II (5), the 2D $k_{on}$ and $k_{off}$ values would be of the order of 0.05 $\mu m^2 s^{-1}$ and 250 $s^{-1}$, respectively, for wild-type CD4/pMHC II interactions.

With [CD4] = 170 molecules/$\mu m^2$ and $k_{on}$ = 0.05 $\mu m^2 s^{-1}$, the number of CD4 binding events per second for an individual pMHC II molecule would be around 9 (see Eq. **S7**). If it again is assumed that 40% of the CD4 molecules are coupled with Lck (41), and that between 2% and 40% of the CD4-Lck are constitutively active (42, 43), this corresponds to each individual pMHC II molecule binding a constitutively active CD4-Lck, on the order of 0.1 to 1 times per second. It was recently suggested that "kinetic-proofreading", a mechanism proposed to allow the TCR to distinguish between pMHC of differing antigenic quality, may rely on the sampling of many CD4 molecules (9). Although the values for $k_{on}$ and $k_{off}$ for the CD4/pMHC II interaction are only estimates, it is feasible that the relatively large $k_{on}$ value, makes it possible for each pMHC II to interact with multiple CD4 ligands during its time in the cell-cell contact. This would be important if only a fraction of the CD4 molecules are associated with Lck.

## SI Materials and Methods – Section 1. 3D affinity

**Cells and protein expression.** HEK 293T cells were maintained in RPMI 1640 media supplemented with 10% heat inactivated fetal calf serum, 1% penicillin/streptomycin (50 IU/ml and 50 μg/ml) and 1% glutamine. The HEK 293T cells were transfected using calcium phosphate precipitation to express pMHC II molecules. Briefly, $0.5 \times 10^6$ cells were transfected with 0.5 μg of each alpha and beta chain construct, and expression was confirmed by fluorescence-activated cell sorting (FACS) analysis using an anti-HLA-DR-phycoerythrin (L243 clone) monoclonal antibody.

**Construction of HLA-peptide constructs and expression.** The DRA*01 sequence was cloned into the pcDNA3.1 Hygromycin expression vector (Invitrogen). The DRB1*01:01 sequence was cloned into the pEGFP-N1 expression vector (Clontech Laboratories) such that the EGFP domain was continuous with the C-terminal cytoplasmic tail. In addition, the Influenza Hemaglutinin (HA) peptide (residues 307-318: PKYVKQNTLKLA) was covalently tagged to the N-terminus via a 12 amino acid Gly-Gly-Ser repeat, and the DRB3*01:01:02:01 leader sequence preceded the peptide (see Fig. S4*A*). Site specific mutations were introduced via two stage over-lap PCR. The biotinylated DR1/HA complex was produced as described previously for HLA-DRB1*04:01/HA (35). Four biotinylated HLA-peptide complexes (34, 35) were used in the solution binding assays studies: DR1/HA (residues 307-318:PKYVKQNTLKLA), DR2/MBP (residues 85-99:ENPVVHFFKNIVTPR), DR4/EBV (residues 627-641:TGGVYHFVKKHVHES) and A24/Den2 (residues 555-

564:INYADRRWCF). The A24/Den2 complex was a kind gift from Prof. Tao Dong, Weatherall Institute of Molecular Medicine, University of Oxford, UK.

**CD4 expression and biotinylation.** sCD4 protein was produced as described previously (18) but expressed with a tag comprising a biotinylation sequence (GLNDIFEAQKIEWHE; sCD4-BirA). sCD4-BirA was biotinylated using an Avidity Biotinylation kit. Briefly, sCD4-BirA protein in 3.5 ml biotinylation buffer (20 mM Tris, pH 7.5, 25 mM NaCl, 7.5 mM $MgCl_2$) was incubated with 400 µl Biomix A (0.5 M bicine buffer, pH 8.3), 400 µl Biomix B (100 mM ATP, 100 mM MgOAc, 500 µM biotin), 100 µl d-biotin (500 µM) and 7 µl BirA enzyme (1 mg/ml) at room temperature for 3.5 hours. The protein was purified by FPLC using 150 mM NaCl, 20 mM Tris (pH 8) buffer through a Sephadex-75 column. The protein was concentrated using Centricon-30 (Amicon) at 1700xg to a final concentration of 1 mg/ml, achieving approximately 60% yield. The control soluble recombinant protein used for ™ studies was a rat CD48-CD4 chimera (rCD48-CD4), containing CD4 domains 3 and 4 and CD48 extracellular domains; this was expressed and biotinylated as previously described (23).

**CD4 tetramer and bead formation.** CD4 biotinylated protein (sCD4biot) was mixed with streptavidin-PE (Molecular Bioprobes) in a 4:1 molar ratio, and tetramers were allowed to form for at least 16 hours at 4 °C. The concentration of the tetramer is given as the concentration of CD4-biotin protein in the sample. To generate CD4-coated beads 10 µg sCD4biot was incubated with $6.7\times10^6$ magnetic streptavidin beads M-280 (Dynal biotech). Streptavidin beads were washed five times in cold PBS and were then incubated with CD4-biotin protein overnight at 4 °C; unbound protein was removed by washing the beads five times with cold PBS.

**SPR measurements.** HIV-1 IIIB gp120 (bac) was from Immuno Diagnostics, supplied by the Centralized Facility for AIDS Reagents supported by EU Programme EVA/MRC and the UK Medical Research Council. CD4 specific antibodies were RPA-T4 (BD biosciences) and ADP318 (Evans Medical Ltd). For the experiments where soluble CD4 was added to the solution, Biacore™ flowcells were coated with streptavidin and biotinylated pMHC molecules were immobilized as follows: DR1/HA at 1600 RU, DR2/MBP at 1750 RU, DR4/EBV at 1840 RU and A24/Den2 as negative control at 1600-1900 RU. Experiments were also made where sCD4biot was immobilized onto streptavidin coated sensor surfaces. For measurement of the affinities between rat CD2 and wild-type and Q40R-mutated rat CD48 (rCD48), a histidine-tagged form of rat CD2 expressed in Chinese hamster ovary cells (44) was injected over ~1200 RU of immobilized biotinylated wild-type and mutant rCD48-CD4 proteins produced as described previously (23).

**CD4-bead binding to pMHC+ 293T cells.** HEK 293T cells were transiently transfected by calcium phosphate precipitation with alpha and beta chain constructs to express wild type (WT) or mutant HA-DR1-GFP molecules, or gp120-GFP controls. Cells were removed from the flask using trypsin/EDTA and washed twice in cold PBS/2% fetal calf serum two days post transfection. $3\times10^6$ cells in 500 µl PBS were incubated with $6.7\times10^6$ CD4 beads on ice for 1.5 hours with gentle agitation, then the bead/cell conjugates were isolated using a Dynal MCP magnetic bead sorter, and resuspended in PBS/2% formaldehyde. Cells were either viewed by fluorescence microscopy and counted in duplicate microscope fields or absolute numbers of cells recovered were determined using a hemocytometer. Alternatively, CD4-coated magnetic

beads were added to HEK 293T cells adhered to wells, and after washing in PBS, bead-bound transfected cells were visualized using immunofluorescence microscopy.

**FACS measurements.** Cells were washed in 5% fetal calf serum/PBS 2 days post transfection and incubated with 20 mg/ml CD4-tetramer, or were stained for DR1 expression using anti-HLA-DR-phycoerythrin (PE) monoclonal antibody (L243 clone), at 4 °C for 30 minutes. Cells were then washed in 0.1% azide/PBS and fixed in 2% formaldehyde/PBS for FACS acquisition. Figure S4*B* (*left*) shows a clear correlation between the amount of WT HA-DR1-GFP and the binding of anti-DR antibody, whereas no binding of anti-DR antibody is observed when gp120-GFP is expressed. When CD4-tetramers were added to the cells expressing WT HA-DR1-GFP no binding of CD4 was observed, whereas strong binding of the CD4-tetramers was observed for cells expressing gp120-GFP (see Fig. S4*B* (*right*)).

## SI Materials and Methods – Section 2. 2D affinity

**Cleaning of substrates.** A glass slide (size no. 1: 0.13 mm in thickness, VWR International) was cleaned in a (3:1 by volume) mixture of concentrated sulfuric acid (>95%; Fisher Scientific) and 30% hydrogen peroxide (100 vols; Breckland Scientific Supplies) for >3 hrs. The sample was then thoroughly rinsed with Milli Q™ water (Millipore) and dried with nitrogen gas after which the glass slide was treated with Ar plasma for 10 min (PDC-002; Harrick Plasma). A silicone isolator (JTR12R-2.0; Grace Bio Labs) was placed on the glass slide following the manufacturer's instructions, to provide a well for the experiments.

**Vesicle preparation.** Lipid vesicles were prepared by extrusion through a 50 nm membrane (Whatman) using an Avanti Mini-Extruder (Avanti Polar Lipids). The vesicles consisted of 1-palmitoyl-2-oleoyl-*sn*-glycero-3-phosphocholine (POPC) from Avanti Polar Lipids with either 5 wt% or 10 wt% of 1,2-dioleoyl-*sn*-glycero-3-[(N-(5-amino-1-carboxypentyl)iminodiacetic acid)succinyl] (Nickel salt) (DGS-NTA; Avanti Polar Lipids). The buffer solution used in all experiments was a mixture of 150 mM NaCl (Breckland Scientific Supplies) and 10 mM tris[hydroxymethyl]aminomethane (TRIS; Pharmacia Biotech), with a pH of 8.0 (TRIS-buffer). The buffer solution was filtered through a 0.2 μm membrane (AnaChem) before use.

**Formation of lipid bilayers.** An SLB was formed by placing a 20 μl drop of the vesicle solution in the wells and leaving it for 30-60 minutes before rinsing. The vesicle solution containing 10 wt% DGS-NTA was used for the CD4/pMHC II measurements, whereas the vesicle solution with 5 wt% DGS-NTA was used for the rat CD2/CD48 measurements. After formation of the SLB the buffer solution was exchanged with either of the two protein mixtures:

(i) human CD2 (containing a polyhistidine tag and labelled with Alexa Fluor® 488) and human CD4 (containing a polyhistidine tag and labelled with Alexa Fluor® 647) or

(ii) human CD58 (containing a polyhistidine tag and labelled with Alexa Fluor® 647) and rat CD2 (containing a polyhistidine tag and labelled with Alexa Fluor® 488),

depending on the measurements. The concentrations of the protein solutions were chosen to achieve a final surface coverage after 1 hr of incubation of:

(i) ~400 molecules/$\mu m^2$ for human CD2 and 400-4000 molecules/$\mu m^2$ for CD4 and

(ii) ~100 molecules/$\mu m^2$ for human CD58 and 35-1600 molecules/$\mu m^2$ for rat CD2,

measured using fluorescence correlation spectroscopy (FCS) (45). An SLB containing a known amount of fluorescently-labelled lipids (0.01 wt% Oregon Green® 488 1,2-dihexadecanoyl-*sn*-glycero-3-phosphoethanolamine; Invitrogen) was used to calibrate the 488 nm beam in the FCS. Different SLBs containing mixtures of streptavidin conjugated with Oregon Green® 488 or Alexa Fluor® 647 (Invitrogen) were used together with the calibrated value for the 488 nm beam to calibrate the 633 nm beam for the concentration measurements of the 647-labelled proteins.

**Cells.** B cells or transfected Jurkat cells were added to the wells with the protein-coupled SLBs. The cells used for the CD4/pMHC II measurements were Raji B-cells, maintained in B-cell medium: RPMI 1640 medium (Invitrogen) supplemented with 10% heat-inactivated fetal bovine serum (HyClone; Thermo-Scientific), 1% L-Glutamine (200 mM; Invitrogen), 1% HEPES solution (Sigma), 1% sodium pyruvate (100 mM; Invitrogen), 1% penicillin/streptomycin (100x; Invitrogen), and kept in an incubator at 37 °C in a humidified atmosphere with 5% $CO_2$. Jurkat cells transfected with the protein CD48, either WT or the weakly binding mutant Q40R, were also maintained in B-cell medium. Before each measurement the cells were resuspended in TRIS-buffer and directly added to the SLB where they were allowed to settle and bind to the proteins in the SLB for ~60 minutes before imaging. For the measurements at 37 °C the SLB was placed in a temperature control system on the microscope where it was heated, and maintained at, 37 °C before adding the cells (also at 37 °C) and imaging.

**Flow Cytometry and Quantibrite analysis.** In order to obtain the number of different membrane proteins per cell the cells were first washed and resuspended in phosphate buffered saline containing 0.05% $NaN_3$ at a concentration of $0.5\times10^6$ cells/ml. Staining was performed by incubation of the cells on ice for 45 minutes with saturating concentrations of PE-conjugated monoclonal antibodies to the following antigens: human CD4 (clone RPA-T4; cat. no. 12-0049-42, eBioscience), anti-HLA-DR (clone L243; cat. no. 12-9952-42, eBioscience) and rat CD48 (clone OX45; cat. no. 204206, Biolegend). After washing, the cells were analyzed by flow cytometry on a Cyan ADP™ (Beckman Coulter) alongside with Quantibrite™ PE beads (BD Bioscience). A calibration curve was generated from four different concentrations of beads with R-PE covalently attached. The calibration curve was used to determine the amount of membrane proteins per cell from the geometric mean of the fluorescence intensity according to the manufacturer's instructions.

**The microscope setup.** The fluorescence imaging was performed in TIRF-mode with an inverted Nikon Eclipse TE200 microscope (Nikon Corporation), using a Photometrics Cascade II:512 EMCCD camera (Photometrics), and a 60× magnification (Plan Apo TIRF, NA = 1.45) oil immersion objective (Nikon Corporation). The acquired images consisted of 512×512 pixels with a pixel size of 0.11×0.11 μm in the sample plane. Using a Dual-View DV2 two-channel, simultaneous-imaging system (Photometrics) the left half of this image corresponded

to the 647 nm fluorescence and the right half to the 488 nm fluorescence, thus allowing for simultaneous imaging of the sample with two wavelengths. A Cyan diode laser operating at a wavelength of 488 nm (model no. PC13589; Spectra Physics) and a HeNe laser operating at 633 nm (model no. 25LHP991230, Melles Griot) were used for illumination. The images were acquired with an exposure time of 100 ms, and 10 images were acquired and averaged for each image.

**Zhu-Golan analysis.** Images of approximately 50 different cells were acquired for each SLB. These images were normalized using an image of the SLB without any cells to compensate for uneven illumination. The intensities in the SLB were converted into surface coverage of proteins using the data obtained from the FCS measurements. The contact region for each cell was first manually selected by a polygon in the human CD2 (rat CD2 for the Jurkat measurements) fluorescence images, leaving sufficient space between the contact region and the polygon border to allow the intensity at the polygon border to be used to normalize the intensity in the contact region. This was achieved by fitting a plane to the intensity on the polygon border, which was then used to normalize the intensity in the contact region. The normalized intensity values within the polygon where subjected to a threshold (intensities larger than 1/3 the maximum intensity in the polygon) to define the contact region under the cell. Averaging the intensity in the contact region gave $B^*/F^*$. The amount of accumulated protein in the contact was obtained by multiplying $B^*/F^*$ with the obtained background intensity outside of the cell contact region, $F^*$. The same masks for the contact region as obtained for the human CD2 images were used to analyze CD4. The area of each cell was obtained from a bright-field image of the cell, where the cell was manually encircled with a polygon and the area of the cell was calculated as 7.2 times the area of this region (16). Dividing the area of the contact region under the cell with the cell area resulted in an estimate of $p$ for each contact.

The data was next analyzed to provide a single averaged value of $B\times p$, $S_{\text{cell}}$ and $B/F$ for each SLB. To avoid analyzing cells where the threshold had produced too-small contact regions, the cells with the lowest values of $p$ were removed from the analysis (the lowest 10% was removed). All data for $B^*/F^*$ was plotted vs $B^*\times p$ and fitted to the expression:

$$y = c_1(x < c_2) + (c_3(x - c_2) + c_1)(x > c_2) \qquad \textbf{[S20]}$$

where $c_1$, $c_2$ and $c_3$ are parameters to be fitted (see Fig. S5). Since the contact area fraction, $p$, is of similar magnitude for different B cells binding to the CD4-SLB (mean value of 4% with a standard deviation of 1%), as is the density of ligands in the SLB, $F^*$, the ratio $B^*/F^*$ is expected to vary approximately linearly with $B^*\times p$. However, this is not the case observed experimentally for CD4 binding pMHC II as seen in Fig. S5, where the ratio $B^*/F^*$ is initially constant at a value $c_1 \approx -0.25$, before it starts to increase linearly with $B^*\times p$ at $B^*\times p = c_2 \approx -3$. This can be interpreted as the B cells with $B^*/F^* = -0.25$ are not accumulating CD4 in the contact, and the value $(B^*/F^*)_0 = -0.25$ therefore corresponds to the depletion of free CD4 beneath the cell when CD4 is not binding pMHC II molecules on the B cell. Only data points where $B^*\times p$ are above $c_2$ were therefore used to obtain $B/F$ and $B$ using Eqs. **S2** and **S4** with $(B^*/F^*)_0 = c_1$. For the rat CD2/CD48 measurements $c_1 = -0.20$ and $c_2 = 0$ was assumed, estimated from the average value of $B^*/F^*$ for non-binding Alexa Fluor® 647 labelled rat CD2

in the contact between an SLB and a B cell anchored to the SLB with human CD2 (see Fig. S6*B*).

Compensating for bleed through between the 488- and the 647-channel did not yield significantly different values for the data, even though a higher intensity in the contact area due to bleed through from the 488-channel could be observed at, in particular, low concentrations of CD4 in the SLB. However, since this will also be the case for $(B^*/F^*)_0$ this largely cancels out the effect of the bleed through from the corrected plots of $B/F$.

The data for $B/F$ vs $B\times p$ was next fitted to Eq. **S1**, to obtain $K_d$. Values for $N_t$ was estimated from FACS-based measurements and $S_{cell}$ from bright-field images as described above. The parameter $f$ was further set to 1, corresponding to all receptors on the cells being mobile.

**Photobleaching measurements.** For the fluorescence recovery after photobleaching (FRAP) measurements, a set of pre-bleach images were first acquired after which a negative lens was positioned in the beam path to cancel out the effect of the Köhler lens in the microscope and focus the laser beam into a small region at the centre of the sample. The photobleaching rate of the sample was increased by removing some of the ND filters in the laser beam path during the bleaching step, thus illuminating the sample with higher intensity during bleaching. After a few seconds the ND filters were put back and the negative lens removed. The recovery of CD4 was imaged with time-lapse acquisition.

Measurements were made both in the SLB/cell contact and outside this region to estimate the diffusivity of CD4 outside the contact. The SLB contained approximately 600 molecules/μm$^2$ of CD4 in all experiments. The intensity after photobleaching had a Gaussian intensity profile:

$$I_r(r,t) = I_0\left[1 - K\exp\left(-r^2/w^2\right)\right] \qquad \textbf{[S21]}$$

where $I_0$ is the intensity before bleaching, $K$ the relative amount of bleaching, $r$ the distance to the centre of the bleached area and $w$ the Gaussian radius of this area. The intensity was normalized to the value before bleaching and subsequently integrated within a circle of radius $R = w/2^{1/2}$. The diffusivity of CD4 was estimated by fitting the integrated intensity to (46):

$$I(t) = \alpha\left[1 - \frac{w^2}{R^2}K\left(1 - \exp\left(-\frac{R^2}{w^2 + 4Dt}\right)\right)\right] \qquad \textbf{[S22]}$$

where $\alpha$, $K$ and $D$ are parameters to be fitted, $D$ is the diffusivity and $R$ was set to $w/2^{1/2}$.

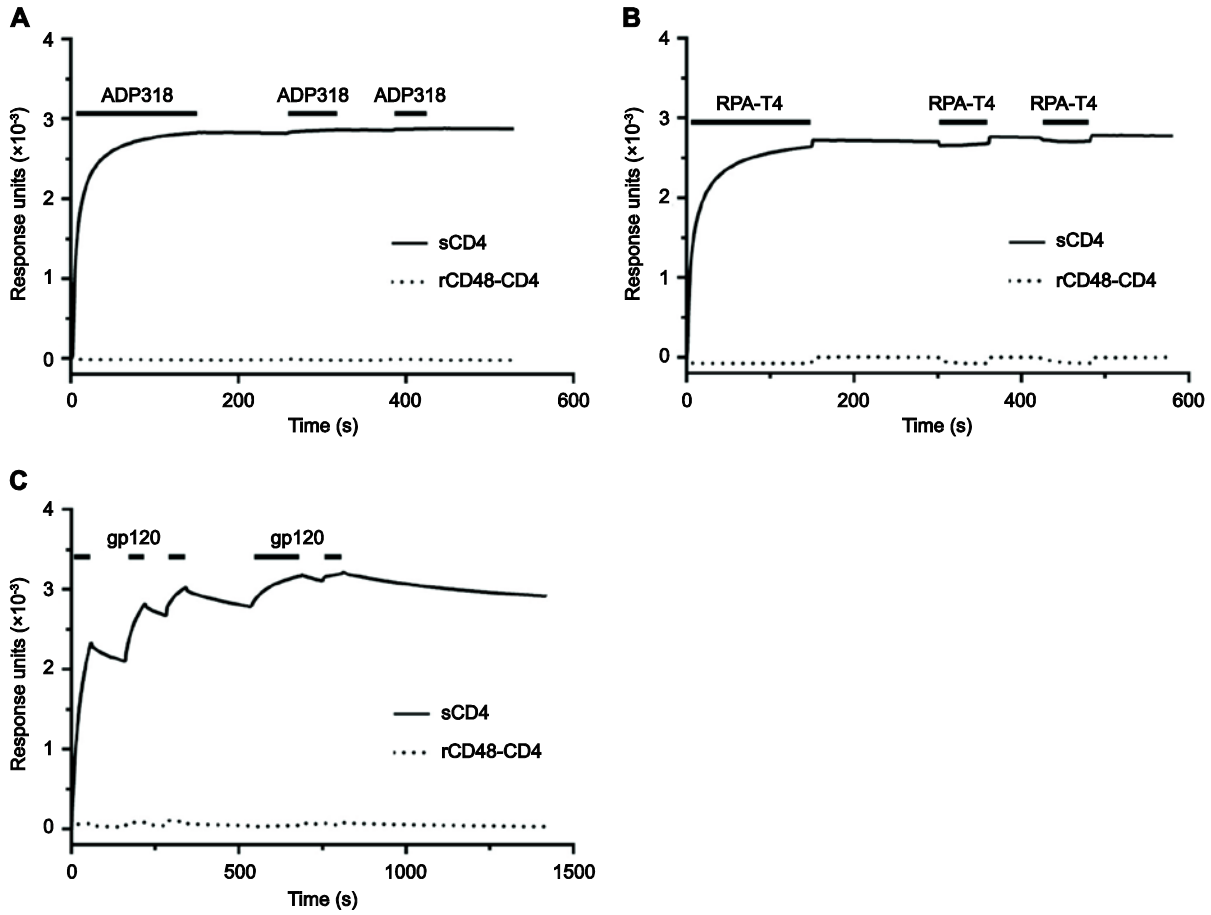


**Fig. S1.** The sCD4 is correctly folded. Sensograms showing binding of anti-human CD4 antibodies: (*A*) ADP318, (*B*) RPA-T4 and (*C*) HIV-1 gp120 to a surface coated with sCD4 or with the control protein rCD48-CD4. Sequential injections were done in order to confirm that saturation binding had been reached, so that the "activity" of the CD4 could be calculated.

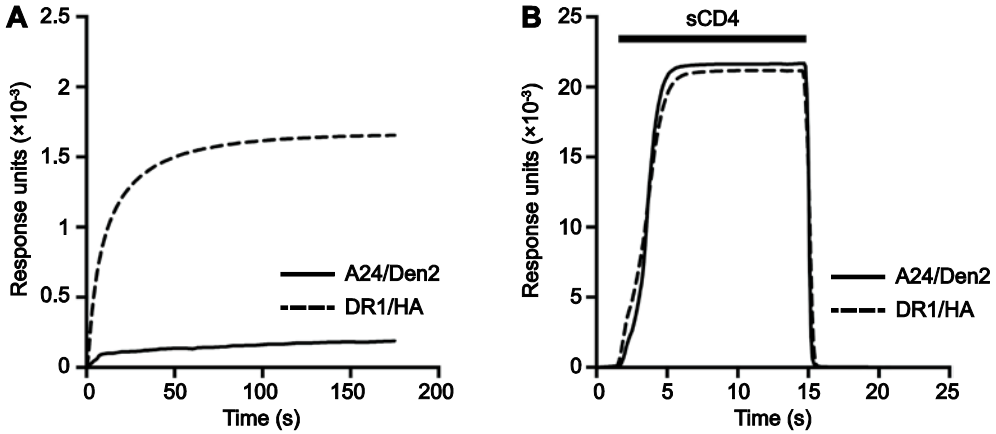


**Fig. S2.** Sensograms showing binding of anti-HLA-DR and sCD4 to pMHC II and pMHC I. (*A*) A sensogram showing injection of saturating levels (0.2 mg/ml) of the anti-HLA-DR antibody L243 over a sensor surface containing immobilized biotinylated pMHC II molecules (DR1/HA; dashed line) or a pMHC I molecule (A24/Den2; solid line) as a control. (*B*) SPR-data showing the response when passing sCD4 at 2.5 mM at 4 °C over biotin-immobilized DR1/HA and A24/Den2.

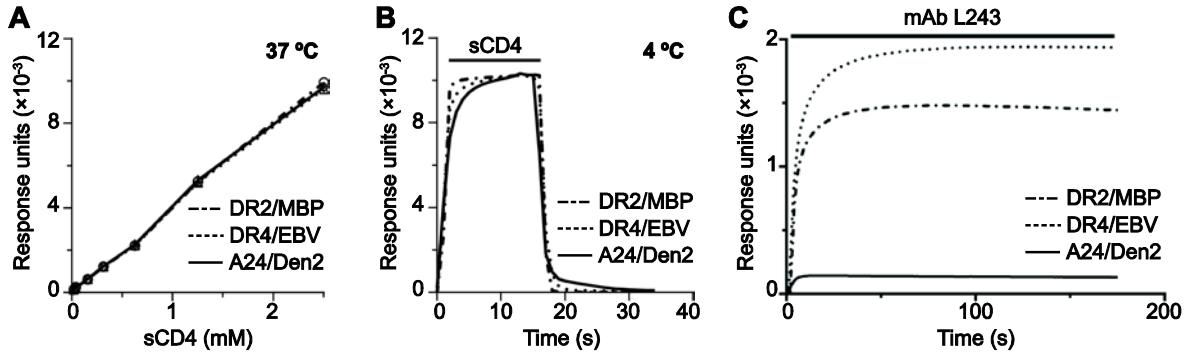


**Fig. S3.** The interaction of CD4 with DR2 and DR4 pMHC II in solution is very weak. (*A*,*B*) SPR-data showing the response when passing sCD4 at a range of concentrations up to 2.5 mM at 37 °C or as a single injection at 2.5 mM at 4 °C over a sensor surface containing immobilized biotinylated DR2/MBP (- · -; ○), DR4/EBV (· · ·; Δ), or a pMHC I molecule A24/Den2 (─; ◊) as a control. (*C*) A sensogram showing injection of saturating levels (0.2 mg/ml) of the anti-HLA-DR antibody L243 over the three samples.

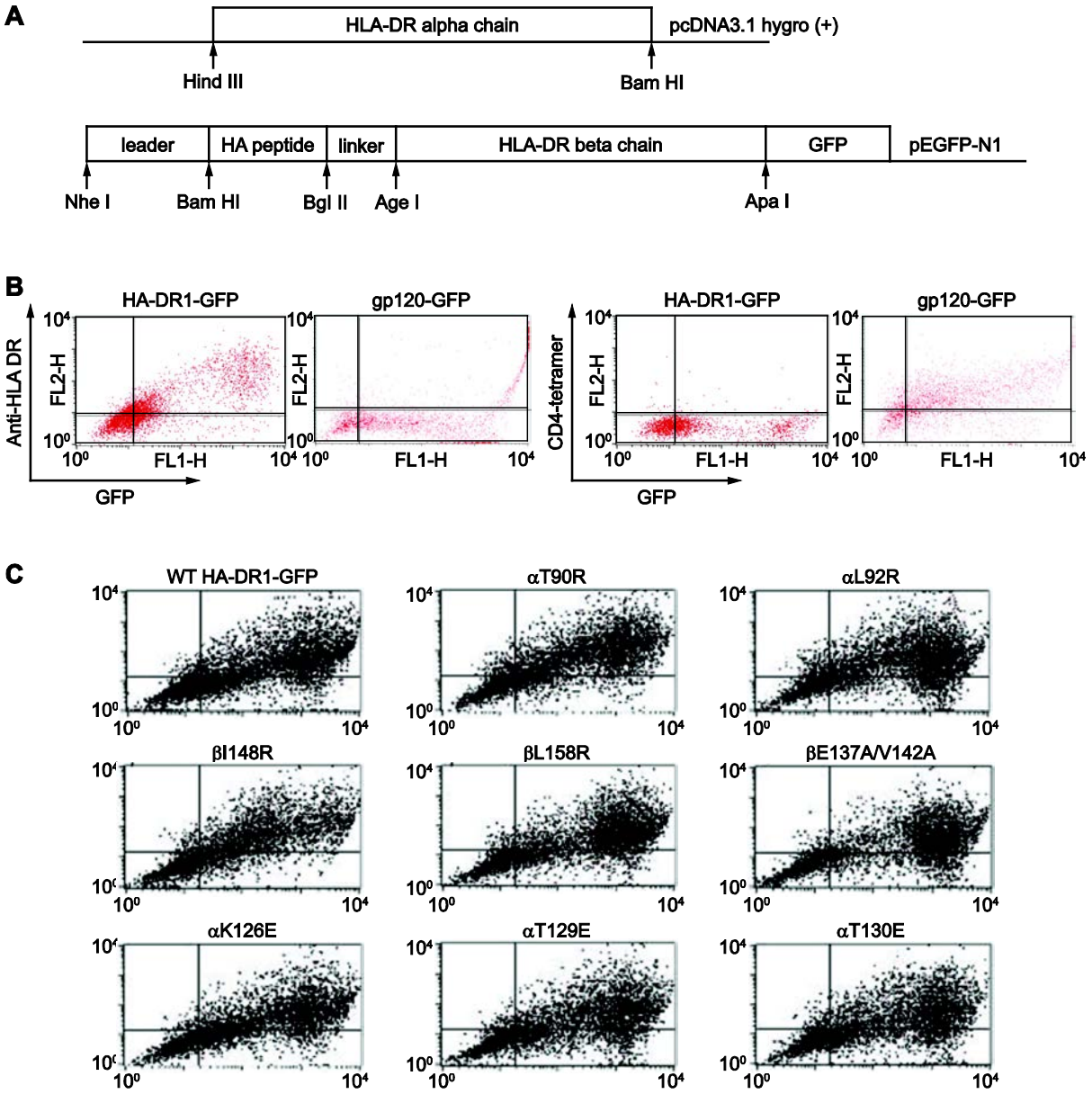


**Fig. S4.** (*A*) Schematic illustration showing the construct used for expression of HA-DR1-GFP. (*B*) FACS data showing binding of (*left*) anti-DR antibodies and (*right*) CD4-tetramers on the *y*-axis vs the GFP intensity on the *x*-axis for HEK 293T cells expressing WT HA-DR1-GFP and gp120-GFP. (*C*) FACS data showing DR1 expression measured using PE-linked anti-HLA-DR (L243) antibody (*y*-axis) vs the amount of fluorescence from GFP linked to the mutant DR1 proteins (*x*-axis).

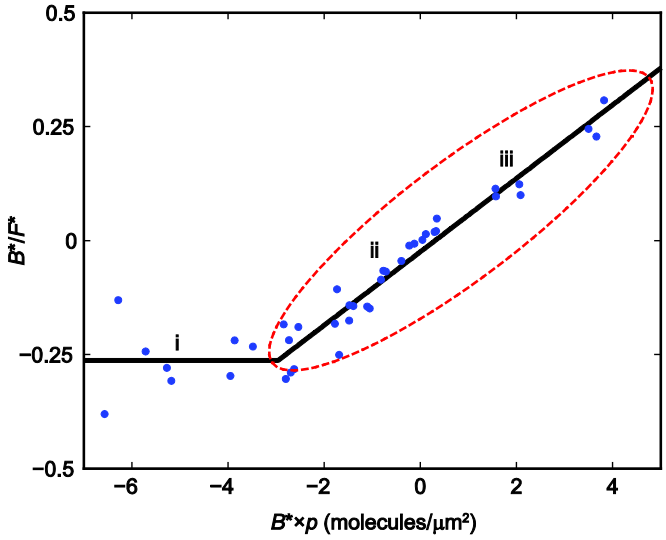


**Fig. S5.** Zhu-Golan plot for a representative SLB showing the apparent amount of bound CD4 in the SLB/B-cell contact for different cells. The numbers i to iii corresponds to the cases shown in Fig. 3. The area encircled with a red, dashed, border is the data points used to obtain an average value for *B*/*F* for each SLB.

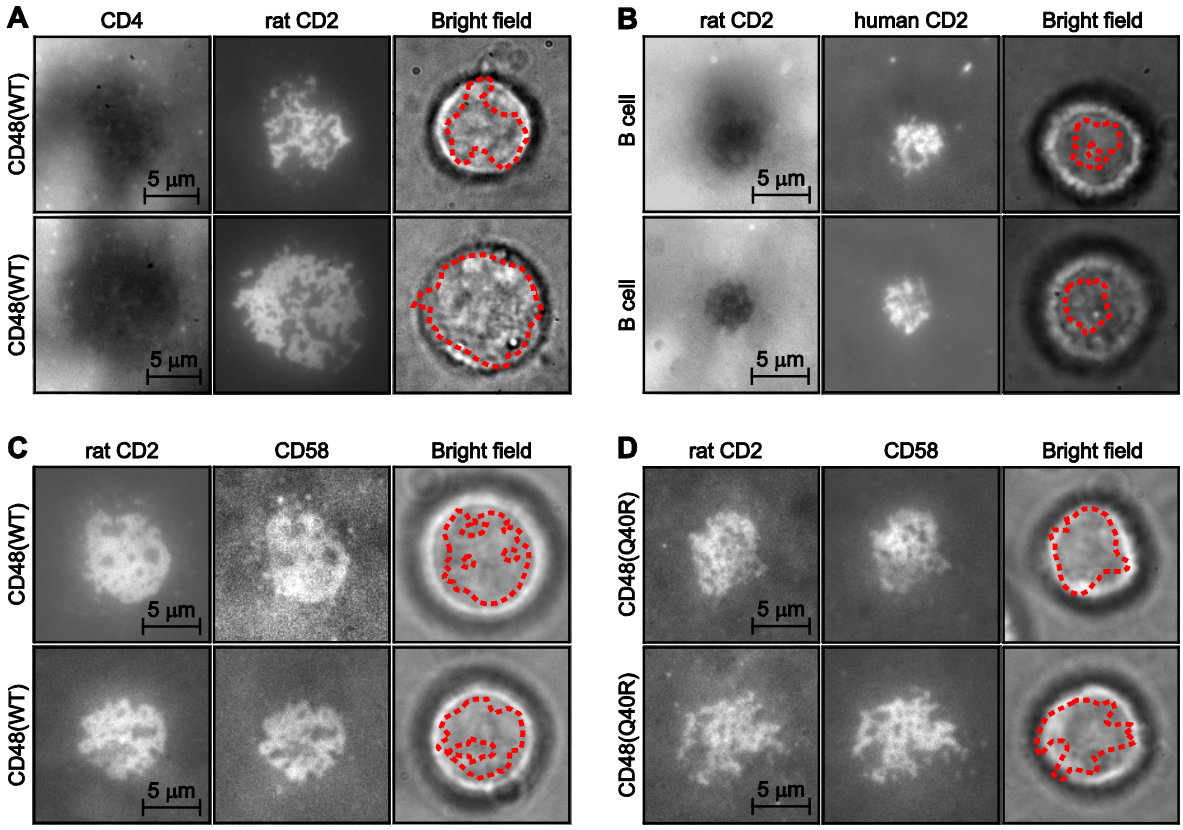


**Fig. S6.** Fluorescence images showing (*A*) depletion of CD4 and accumulation of rat CD2 in the contact to CD48(WT)-transfected Jurkat cells, (*B*) depletion of rat CD2 and accumulation of human CD2 in the contact to B cells, (*C*) accumulation of rat CD2 and human CD58 in the contact to CD48(WT)-transfected Jurkat cells and (*D*) accumulation of rat CD2 and human CD58 in the contact to the weak-binding mutant CD48(Q40R)-transfected Jurkat cells. The dashed line in the bright-field images shows the contour of the SLB/cell contact as obtained from the accumulation in the middle column of images for each case.

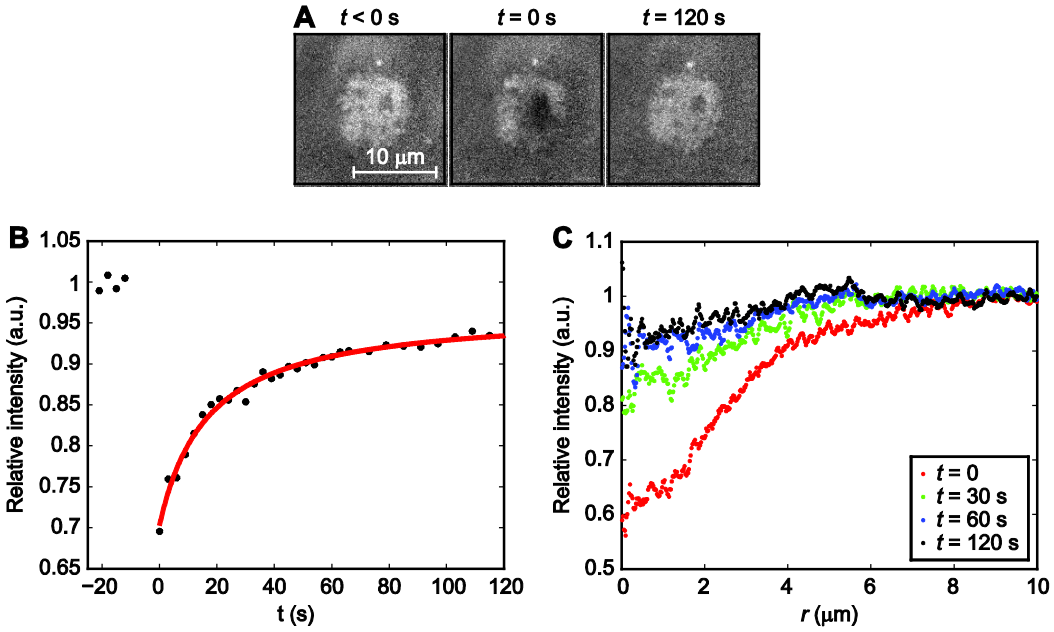


**Fig. S7.** The CD4/pMHC II interaction is dynamic. (*A*) Representative fluorescence images showing fluorescently-labelled CD4 in an SLB/B-cell contact before photobleaching ($t < 0$ s), just after photobleaching ($t = 0$ s) and $t = 120$ s after photobleaching. (*B*) The integrated intensity, $I$, in the centre of the bleached area relative to the value before photobleaching ($t < 0$ s). The solid line is a curve fit of the recovery data at $t \geq 0$ s (see Eq. **S22**). (*C*) Radial intensity line profiles. The radial distance $r = 0$ corresponds to the centre of the bleached region. The intensity is normalized to the value before photobleaching.

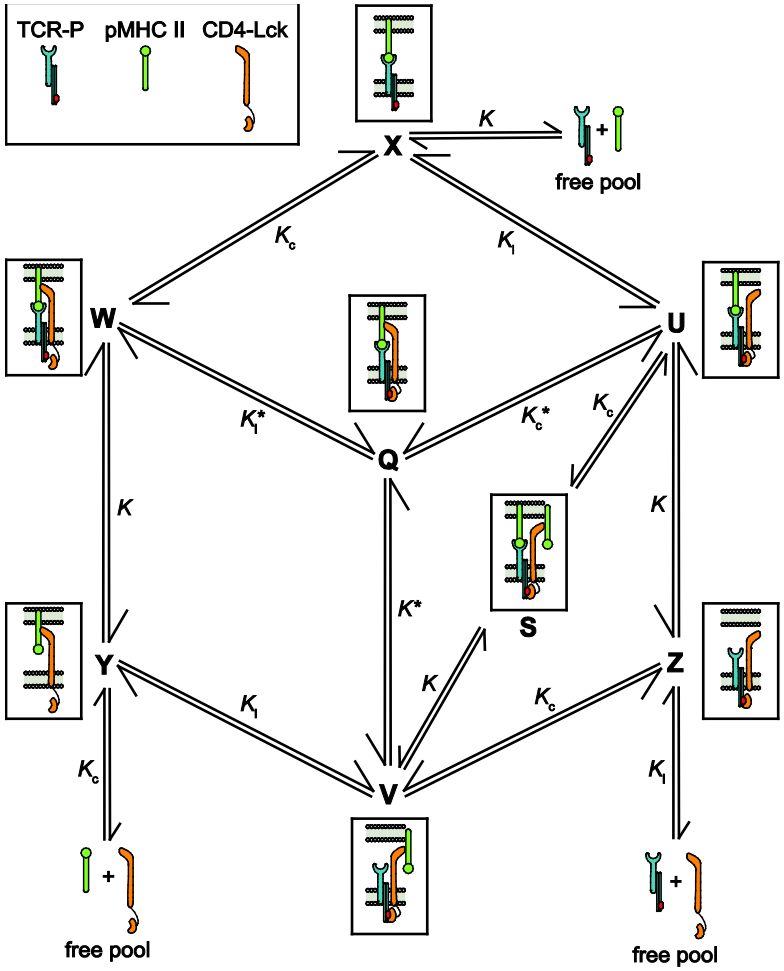


**Fig. S8.** Schematic illustration showing the different states (*X*, *U*, *Q*, *W*, *S*, *Z*, *V* and *Y*) in the kinetic modelling, with the equilibrium constants: $K_c$, $K_l$, $K$, $K_c^*$, $K_l^*$ and $K^*$.

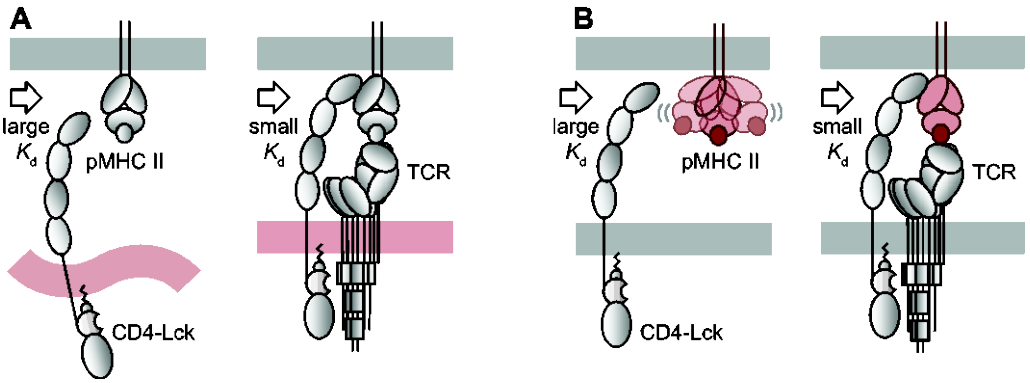


**Fig. S9.** Binding of CD4 to a TCR/pMHC II complex can potentially increase the affinity of CD4 to pMHC II. (*A*) Schematic illustrations showing how binding of pMHC II to TCR can reduce the energy loss associated with membrane fluctuations (47) upon CD4 binding to pMHC II and (*B*) to arrange pMHC II at a suitable distance and position for CD4 binding.

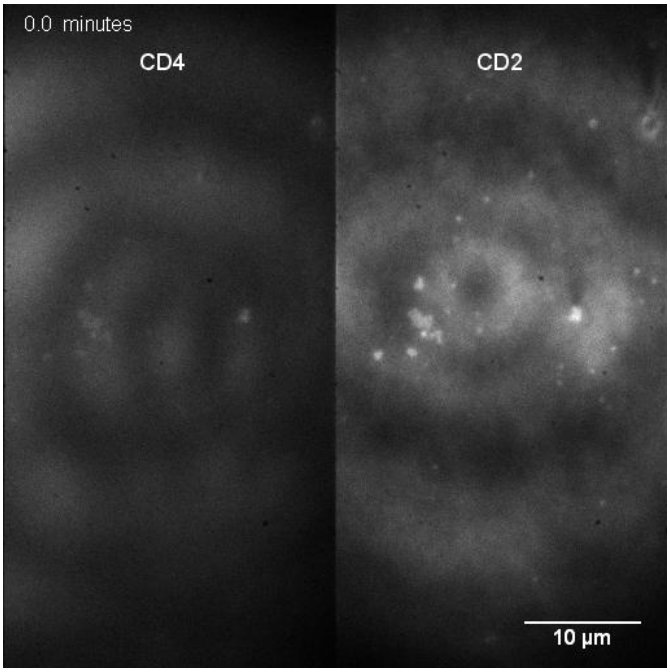


**Still Image for Video S1.** B cells landing and binding to lipid-anchored CD4 and CD2 in an SLB. The SLB contained 900 molecules/$\mu m^2$ of Alexa Fluor® 647-labelled CD4 and 400 molecules/$\mu m^2$ of Alexa Fluor® 488-labelled CD2. The last frame is a bright-field image taken after 57.5 minutes.